Appendix B

Spatial Cross-Correlation of Antarctic Sea Ice and Seabed Topography

Richard D. De Veaux and Michael J. Phelan

Program in Statistics and Operations Research
School of Engineering and Applied Science
Princeton University
Princeton, NJ 08544

We consider a time series of derived sea-ice concentrations as observed about Antarctica by the Nimbus-7 SMMR satellite in 1983. We quantify the degree of spatial cross-correlation between these data and seabed topography. Our approach is to implement a statistical image-processing filter designed to extract local patterns of spatial cross-correlation over the entire sea-ice field as it undergoes daily changes. Throughout the sea ice, we find that large-scale variations in sea-ice concentration correlate systematically with variations in the topography of the seabed. Generally speaking, high concentrations of sea ice occur over deep ocean, whereas areas of encavement, early dissipation and polynya formation develop over topographic features of high elevation. We investigate the latter in detail with respect to the features Maud Rise, Astrid Ridge and the continental shelf in the Cosmonaut and Ross Seas. In each case, we show that an encavement in sea ice, a polynya, or both develops in the vicinity of the feature in question. As we quantify these results in terms of spatial cross-correlation, we infer a potential role for seabed topography in such fluctuations in the sea ice about Antarctica.

INTRODUCTION

We investigate the role of seabed topography in variations in sea-ice concentration as observed about Antarctica. Our analysis covers the entire sea-ice field as it undergoes daily changes as observed by the Nimbus-7 Scanning Multichannel Microwave Radiometer (SMMR) satellite in 1983. The aim is to show that features of the large-scale variability in sea ice correlate systematically with that in seabed topography.

The occurrence of the Maud Rise polynya represents a pronounced example of large-scale variability in Antarctic sea ice. Indeed, this event entailed the development of a large area of open water contained within the sea ice in the vicinity of Maud Rise (2°E, 64°S). *Comiso and Gordon* [1987] drew the apparent connection between the occurrence of this hole and the presence of the topographic feature Maud Rise, suggesting a possible link between seabed topography and variations in sea ice. In fact, based on these qualitative observations, *Gordon and Huber* [1990] implicate topographic features such as a seamount in a hypothesized sequence of events leading to the occurrence of a polynya. Their conjecture is in part an attempt to account for the unexpected occurrence of polynyas over the open ocean. Some such linkage may also be at work in the occurrence of the Cosmonaut polynya as reported by *Comiso and Gordon* [1987].

In addition to open ocean polynyas, such as the one at Maud Rise and in the Cosmonaut Sea, coastal polynyas are also common about Antarctica. They are thought to play a major role in the building of the sea ice during winter, and in this connection researchers including *Zwally, et al.* [1985], *Kurtz and Bromwich* [1985], and *Cavalieri and Martin* [1985] have focused on the importance of katabatic winds in the occurrence and persistence of these polynyas. Nevertheless, characteristics of the seabed may be an important secondary factor because of the influence the seabed has on ocean currents. In particular, *Pillsbury and Jacobs* [1985], *Kurtz and Bromwich* [1985], and *Zwally, et al.* [1985] have each suggested a role for oceanic as well as atmospheric forcing in the life cycle of coastal polynyas, including the one at Terra Nova Bay, Ross Ice Shelf, as well as other localities throughout the coast.

Here we aim to demonstrate quantitatively that variations in Antarctic sea ice occur systematically relative to changes in seabed topography. Our approach is to quantify the degree of spatial cross-correlation between sea-ice concentrations and ocean depth. On the one hand, we have a time series of satellite images depicting three-day averages of sea-ice concentrations in 900-km^2 pixels throughout the sea ice. The data were converted from brightness temperatures, as observed by the Nimbus-7 SMMR satellite, by *Comiso and Zwally* [1989]. On the other hand, we have measurements of the depth of the Antarctic seabed in 36-km^2 pixels, which we have aggregated to the same spatial scale as the sea-ice images. These data are part of the Southern Ocean Atlas and were made available to us through the Lamont-Doherty Geological Observatory at Columbia University. We focus on the local patterns of spatial cross-correlation between the two sets of measurements. Our approach is to implement a statistical image-processing filter designed to extract these patterns over the entire sea-ice field as it undergoes daily changes. The result is a quantitative summary of the degree of local, linear association between ocean depth and sea-ice concentration throughout the field. As we produce these summaries of spatial cross-correlation at every time in the time series, we monitor the derived pattern of linear association as it evolves over the entire year.

The qualitative observations cited above connect the occurrence of polynyas with seabed topography and oceanic forcing. As the first quantitative analysis of the role of seabed topography in sea-ice processes, the present analysis attempts to move these observations toward a more rigorous understanding of the connections noted therein. Our results implicate seabed topography as an important determinant of sea-ice processes such as the occurrence of encavements and polynyas over the open ocean. We discuss their relevance in specific with regard to the theoretical framework for the occurrence of polynyas in *Gordon and Huber* [1990].

2. Data and Methodology

We describe the data and the methodology used in our analysis of Antarctic sea ice. Much of our technology is based on visualization through image analysis, computer animation, and graphical statistical techniques. Some of these tools will be introduced as needed in our results section, but the correlation filter, our principal image processing tool, is described here in detail.

Data. Two sets of data were used in our analysis: one of sea-ice concentrations and one of ocean depths. The data on sea-ice concentrations were obtained from the National Aeronautics and Space Administration's Laboratory for Oceans, Goddard Space Flight Center in Greenbelt, MD. These data consist of a time series of satellite images depicting sea-ice concentrations (% ice) over the Antarctic region during 1983. Each image represents a three-day average of sea-ice concentration taken every other day, so that there is a total of 178 images in the time series. The sea-ice concentrations were converted by *Comiso and Zwally* [1989] from brightness temperatures, emitted from the Earth's surface and atmosphere, as measured from the Nimbus-7 SMMR satellite along its 18 GHz and 37 GHz channels. The satellite has a scanning footprint of about 30 km $\times$ 30 km, so that the sea-ice images consist of a 293 by 293 array of approximately 900-km^2 pixels covering the Antarctic region. For the purpose of our analysis, as a way to estimate missing values and attenuate the effects of synoptic scale weather events, we implemented a temporal filter that replaces each image with its running median of 3 in time.

Figure 1 shows a series of images depicting sea-ice concentrations at a number of days in 1983. The images are depicted in accord with the color key appearing in Exhibit 1. At top left in Figure 1, we begin with an image in early March when the ice is more-or-less at full contraction. In the weeks to follow, the sea ice grows through to its maximal winter extension with the rate of growth being particularly rapid over the Weddell Basin, the Ross Sea, and in the area east of the Ross Sea to the Antarctic Peninsula. By about late August [center in Figure 1], the ice assumes its final extension and shape. To a large extent, the shape of the boundary or outer edge of the sea ice conforms to that of the continent, except for the sharp 'corner' that occurs at about 135°W, 65°N. It remains to account for this feature in terms of ocean depth.

In contrast to the areas of rapid growth mentioned above, the sea ice grows relatively more slowly along the remaining stretches of the Antarctic coast. As is seen in early July [top right in Figure 1], there is an area of weak growth in the Cosmonaut Sea at about 45°E, 65°S, which is in the vicinity of the Cosmonaut polynya as observed by *Comiso and Gordon* [1987]. We focus on this area later in our analysis.

The month of October produces some noticeable variations in sea-ice concentration, particularly those associated with encavements in the vicinity of Maud Rise and in the Ross Sea. These encavements are evident in mid November[lower left in Figure 1] and they manifest as polynyas around mid December [bottom middle in Figure 1]. Thereafter, as the Austral summer approaches, the sea ice dissipates dramatically. As it does so. dissipation occurs earliest and proceeds rapidly over Maud Rise and in the Ross Sea. In contrast, it occurs later and proceeds more slowly in the area stretching eastward from the Cosmonaut Sea to the Ross Sea, in the Weddell Sea, and in the area west of the Antarctic Peninsula.

The data on ocean depth are from the Southern Ocean Atlas and were obtained from the Lamont-Doherty Geological Observatory of Columbia University, Palisades, NY. The data consist of a single image depicting the topography of the seabed lying beneath the Southern Ocean. The bathymetric measurements were obtained from a variety of sources, including sounding from ships, at a much finer spatial resolution than appears in the sea-ice images. We thus converted these data to an image of the same spatial resolution as the images of sea ice, yielding a bathymetry image depicting the average depth of the ocean over a 293 by 293 array of 900-km^2 pixels covering the Antarctic region. There is some loss of information entailed in this aggregation of measurements, but for our purposes here the computational advantages in doing so seem to far outweigh the potential loss.

Figure 2 shows the bathymetry image depicting the depth of ocean about Antarctica. The depths being depicted range approximately between 1 km and 5 km, where the color key appears in Exhibit 1. Using this image, we urge the reader to locate, for example, Maud Rise, Kainan Maru Seamount, and the slope of the continental shelf in the Ross Sea. We will analyze these areas in some detail later.

Correlation Filter. Recall that our objective is to quantify the influence of seabed topography on sea-ice behavior. The problem is one of extracting the relevant information from the time series of sea-ice images, where here we focus on the pattern of local cross-correlation between sea-ice concentration and ocean depth. Our approach combines the use of a statistical image-processing filter and computer animation, where our analyses are performed using an IRIS-4D workstation to execute a combination of user-designed procedures written in the programming language C, the Princeton Graphics Tools, and the data-analysis environment of S [see *Becker, et al.* [1988]].

The statistical image-processing filter referred to above was designed to determine the degree of local cross-correlation between sea-ice concentration and ocean depth. The procedure creates a time series of correlation images depicting the spatial pattern of this correlation throughout the sea ice, where each is determined as follows. Fix a day in the time series of sea-ice images, and consider the pair of images given by the sea-ice image of that day and the bathymetry image. The filter maps this pair of images into a third image depicting the spatial cross-correlation between the two. To do so, we fix a window size for the filter of 11 $\times$ 11 pixels, representing an area of about 109,000 km^2 or 330 km $\times$ 330 km. This area covers variation in sea ice at the approximate scale of the Maud Rise (about 92,000 km^2) and the Cosmonaut (about 137,700 km^2) polynyas [see *Comiso and Gordon* [1987]]. Moreover, as Figure 3 illustrates, there is little evidence of cross-correlation at the scale of the entire Antarctic region. The scatter plot of sea-ice concentration versus ocean depth over the entire region yields no evidence of simple structure, necessitating the search for such structure at smaller scales. The scale chosen here also keeps the computational burdens to a reasonable level.

Given the window size, the correlation image is then determined as follows. The filter passes the window simultaneously over the pair of images by moving its center from pixel to pixel across the entire 293 by 293 array of them. Suppose that the window is centered at the ijth pixels in the array, where $1 \leq i, j \leq 293$. Ignoring for the moment pixels near the boundaries of the image, this determines 121 (i.e. 11^2) pairs of measurements, where each pair consists of the ocean depth and the sea-ice concentration measured at a given

pixel location contained within the window. The value at the ijth pixel in the correlation image is then the correlation coefficient determined by these pairs, giving the local cross-correlation between ice concentration and ocean depth. The procedure is carried-out across all pixels and the operations repeated throughout the entire year, thus creating a time series of 178 correlation images depicting the desired patterns of spatial correlation. As pixels near the boundaries of the sea-ice image do not involve sea-ice, we encode these with an arbitrary value in the correlation images.

Next we animate the time series of correlation images, as a way to view the variations in local correlation over the year. While showing the temporal evolution of these patterns, the animation highlights regions of the sea ice field and periods of its life cycle having particularly strong linear association with ocean depth. It turns out that the image-processing filter acts as a feature detector by enhancing interesting, localized patterns of sea-ice variation requiring further attention. We illustrate this point in the results section.

3. Results

We describe our results by presenting a series of graphical displays illustrating the structure of the spatial cross-correlation between the sea ice and ocean depth. Our aim is to highlight interesting features and patterns in these correlations and examine their temporal evolution.

Correlation Images

Recall that our approach is to implement a statistical image-processing filter designed to highlight local patterns in the spatial cross-correlation. Figure 4 displays the correlation images obtained from the sea-ice images of Figure 1, where the color key appears in Exhibit 1. The purpose of these images is to highlight patterns of relatively strong linear association.

To interpret the correlation images, we note that positive correlations indicate the occurrence of decreasing sea-ice concentration in the presence of topographic features of decreasing depth or they indicate the converse. The negative correlations indicate the occurrence of decreasing sea-ice concentration in the presence of topographic features of increasing depth or they indicate the converse. Finally, zero or negligible correlations, which we take to include those coefficients inside of the interval [-0.6, 0.6], indicate the presence of little or no variation in sea ice, topography, or both, or when variations in these are present, they indicate that a linear relationship is an inadequate summary thereof.

A number of interesting features present themselves. The images highlight the occurrence of encavements and polynyas over topographic highs, the presence of edge effects along the outer edge of the ice shelf and over the continental shelf as well, and finally the development and persistence of high concentrations over deep water. The most notable example of the latter occurs in winter in the Weddell Sea, where we find the occurrence and persistence of the highest concentrations of sea ice sitting over this deep sea. Sea-ice concentrations average nearly 100% and the depth averages about 5 km, with there being little or no variation present in either. As depicted in the winter images of Figure 4, the spatial cross-correlations in the Weddell region thus fall within the negligible range.

We next draw attention to the edge effects. As depicted in Figure 4, notice the stretch of negative correlation along the outer edge of the sea ice, where sea-ice concentrations typically decrease and the seabed is increasing in depth. In contrast, depth decreases towards the continental shelf and so does sea-ice concentration, and thus the stretch of positive correlations near the continent. The latter may in part be due to contamination of the sea-ice data near the continent as a result of averaging with the lower emissivity of the land. The former appears to be expected, yet topography may still play a more subtle role in determining the edge of the ice field. We refer to a possible role in determining the ultimate growth and hence the final shape of the field as depicted in the middle row of images in Figure 1. We return to this point in our discussion.

Finally, the correlation images and their animation highlight several features of positive correlation that are visible in Figure 4. In addition to the interior edge effects mentioned above, pronounced features of positive correlation occur in the vicinity of Maud Rise, in the Ross Sea, and along the Antarctic-Pacific and South Scotia Ridges. In each case, encavements or regions of the ice field having low sea-ice concentration occur in the vicinity of topographic highs, where the latter are determined by an orographic feature in the seabed. As may be seen in Figure 1, the 'shape' of each encavement appears to mimic the 'shape' of the orographic feature sitting beneath it. In specific, the Antarctic-Pacific and South-Scotia Ridge encavements manifest the distinctly linear patterns of those ridges, whereas the Maud-Rise encavement manifests the convex shape that outlines the topographic contours of Maud Rise, and the shape of the Ross-Sea encavement manifests that of the continental shelf in the Ross Sea. We thus have a demonstrable coherence between the occurrence of encavements in sea ice and variations in seabed topography, which we explore in more detail next.

Sea-Ice Concentration and Spatial Cross-Correlation Fields in the Three Seas

Here we examine the temporal evolution of the fields of sea-ice concentration and spatial cross-correlation in each of the Weddell Sea, the Ross Sea, and the Cosmonaut Sea. In doing so, we detail the local structure of the spatial cross-correlation between sea-ice concentration and seabed topography. Our aim is to underscore the observation made above that the presence of topographic features of high elevation correlates positively with the occurrence of encavements in sea-ice concentration.

We isolate a rectangular area of study in each of the Weddell, Ross, and Cosmonaut Seas. Table 1 displays the latitude-longitude pairs at the corners of each area. The Weddell and Ross Sea study areas are each about 900 × 1200 km rectangles, whereas the Cosmonaut Sea study area is about a 1500 × 1500 km square. The bathymetric contours depicting seabed topography in each of the study areas appear in Figure 5. Notice, for example, Maud Rise (2°E, 66°S) in the Weddell Sea, Kainan Maru Seamounts (34°E, 66°S) in the Cosmonaut Sea, and the slope of the continental shelf in the Ross Sea. We refer to these and other topographic features below. Finally, we remark that the Weddell Sea and Cosmonaut Sea study areas were chosen to cover the sites of the 1980 Maud Rise and Cosmonaut polynyas as observed by *Comiso and Gordon* [1987] at 2°E, 64°S and 43°E, 66°S, respectively.

Weddell Sea. The principal topographic feature in the Weddell Sea study area is Maud Rise. The presence of this seamount correlates positively with the occurrence of an encavement in sea-ice concentration and the eventual development of a polynya. As a result, Maud Rise localizes the area of earliest and most rapid dissipation of sea ice in the Weddell Sea.

Figure 6 displays the sea-ice concentration and spatial cross-correlation fields in the Weddell Sea study area at a selected number of days in 1983. We begin with conditions on 22 July 1983, when after a period of growth in May, June and early July, the ice covers the study area with essentially 100% sea ice. The exception occurs in the area north of about 60°S, which locates the edge of the ice. These conditions more-or-less persist throughout

August and into early September as depicted on 4 September 1983. Over this period, there is only weak spatial cross-correlation present throughout the study area with the exception being the strong positive cross-correlation in the upper-right corner. The latter seems largely connected with an edge effect whereby decreasing concentrations of ice at the edge of the ice field correlate positively with the rising elevation of the seabed there. As seen in Figure 6, this pattern persists throughout the season until the ice melts, and it may play a role in the early dissipation of this part the field's edge.

The first sign of notable cross-correlation associated with Maud Rise occurs in mid to late September. To wit, consider the pattern of spatial cross-correlation on 20 September 1983 as depicted in Figure 6. Notice the 'band' of positive correlation that wraps about the 'base' of Maud Rise, where the maximum cross-correlations occur to the north of the seamount and reach magnitudes of about 0.7 to 0.8. Having first appeared in early July, this pattern involves decreasing sea-ice concentration in the presence of rising elevation and figures significantly in the development of the Maud-Rise encavement.

The Maud-Rise encavement entails substantial decay in sea-ice concentration in the vicinity of Maud Rise. The temporal evolution of this event is depicted in the remaining panels of Figure 6, displaying conditions on October 2 and 26, November 3, 7, 13 and 19, and December 1, 3, and 7 of 1983. The spatial cross-correlation fields show an expanding area of strong positive cross-correlation about the seamount. This manifests the decaying concentrations of sea ice situated over Maud Rise relative to consistently higher concentrations situated over the surrounding deep ocean. By about 1 December 1983, sea-ice concentrations in the encavement area are in the range of 10% to 15% surrounded by concentrations of 45% and above. According to the operational definition of *Zwally, et al.* [1985], these concentrations are low enough to indicate the presence of a polynya. Indeed, a large hole appears in the ice shelf on 3 December 1983 and localizes an interior area of the ice field of particularly rapid dissipation.

Cosmonaut Sea. The principal topographic features in the Cosmonaut Sea study area are the eastern edge of the Astrid Ridge, the Kainan Maru Seamounts, and the continental shelf lying to the east of the seamounts. The area covers the site of the 1980 Cosmonaut

polynya at 45°E, 65°S. Apparently, the polynya fails to recur there in 1983, but the site does localize an area of weak encavement and of shallow embayment at winter's end. On the other hand, the presence of the Astrid Ridge correlates positively with the occurrence of an encavement and the development of a polynya. For 1983, it thus localizes the area of early and rapid dissipation of sea ice in the Cosmonaut Sea.

Figure 7 displays the sea-ice concentration and spatial cross-correlation fields in the Cosmonaut Sea study area at a selected number of days in 1983. We begin with conditions as they appear on 3 August 1983, which roughly marks the end of the growing season for the sea ice in the Cosmonaut Sea. The edge of the ice runs along 60°S in the upper-right corner of the study area. As the tapering sea-ice concentrations there extend over the deepening waters, an area of strong, negative cross-correlation is generated in the cross-correlation field. This particular feature persists throughout the winter season.

Next consider conditions on 20 September 1983 and 14 October 1983. We draw attention to the band of contours of positive cross-correlation running along the coastline and north along 22.5°E longitude. This separates a field of predominantly negative cross-correlation to its north and east from that of predominantly positive cross-correlation to its south and west. Observe that those contours along the coast cohere apparently with the bathemetric contours of the seabed, having a noticeable 'bulge' in the vicinity of the Kainan Maru Seamounts and the continental shelf lying east of there. Moreover, on 14 October 1983, there is a distinct area of 5% to 10% encavement in sea-ice concentration located at about 15°E, 65°S, which locates the Astrid-Ridge feature of highest elevation and the site of the Astrid-Ridge encavement.

The remaining panels in Figure 7 depict the temporal evolution of the conditions described above. First consider those depicting conditions on 5, 17, and 19 November 1983. Observe that the split pattern of positive and negative cross-correlation described above persists at these times. There is, however, no obvious encavement developing at the historical site of the Cosmonaut polynya, but an embayment appears to develop there later. In contrast, there is an obvious encavement centered at about 17.5°E, 64°S, representing the deepening of the Astrid-Ridge encavement mentioned above. As seen on November 23,

25, and 27 and December 3 and 7 of 1983, the deepening trend continues as the Astrid-Ridge encavement opens to a polynya and, along with the embayment cited above, localizes an area of rapid dissipation in the Cosmonaut Sea.

Ross Sea. The principal topographic feature in the Ross Sea study area is the continental shelf. The waters run about 400 km deep there, being separated from 4,000 km deep waters in the northeastern part of the study area by the slope of the continental shelf. A gradient of similar structure manifests in the sea-ice concentration field, where high concentrations persist over the deep waters while an encavement develops over the continental shelf. The latter localizes an area of rapid dissipation and the development of a polynya at winter's end.

Figure 8 displays the sea-ice concentration and spatial cross-correlation fields in the Ross Sea study area at selected days in 1983. We begin with conditions on 4 March 1983, when the Ross Sea ice field is in an early stage of growth. As expected during this period when relatively low concentrations of sea ice push out over the study area, a pattern of positive and one of negative correlation occurs over the shallow and the deep waters of the study area, respectively. The cross-correlation contours marking the gradient of separation between the two apparently cohere to those of the continental slope itself. As the ice continues to grow, this pattern persists and is still present on 24 March 1983, for example, as depicted in Figure 8.

Next consider conditions on 13 April 1983, when the edge of the ice field extends just north of 70°S latitude. Otherwise, sea ice covers the study area with concentrations of about 90% to 95%. First observe the pattern of strong, positive cross-correlation lying in the southwest between 74°S and 76°S. According to the sea-ice concentration field there, there is a relative encavement developing over the continental shelf as the first sign of the Ross-Sea encavement. At the same time, there is another encavement situated over the 'foothills' of the Antarctic-Pacific Ridge, which accounts for the pattern of strong, positive correlation lying to the northeast above 70°S. Both encavements persist, for example, on 27 April and 11 May of 1983, well within the period when the sea ice completely covers the study area.

As part of the cross-correlation pattern described above, there are 'linear' patterns of cross-correlation contours that appear to localizes and mimic similar patterns in the bathymetric contours of the seabed: one coherent with those of the continental slope, the other with those of the foothills of the Antarctic-Pacific Ridge. These, of course, separate the alternating areas of positive and negative cross-correlation described above. As seen in Figure 8, these conditions prevail on June 6 and 22 and July 6 and 22 of 1983, illustrating that they remain stable for several weeks despite the potential for synoptic-scale weather effects to induce departures from the trend. In August, however, the conditions described above change. For example, consider conditions on 15 August 1983 as depicted in Figure 8. The spatial cross-correlation field is dominated by positive cross-correlation of strong magnitude. Throughout the study area, the sea-ice concentration field shows that sea-ice concentrations of high percentage sit over deep waters while relatively lower percentage concentrations sit over the shallows. The latter includes the Ross-Sea encavement developing over the continental shelf.

This new trend continues through September and early October, when the Austral spring sets in and magnifies the Ross-Sea encavement. For example, consider the conditions on 14 October 1983. A substantial encavement in sea-ice concentration occurs in the vicinity of 185°E, 75°S, where local concentrations of sea ice dip to about 70% or 10% to 20% lower than the surrounding area. This Ross-Sea encavement sits over the shallowest waters in the study area, producing a peak of positive cross-correlation over the continental shelf. Then on 19 November 1983, local concentrations of sea ice fall as low as 30% in the vicinity of 180°E, 74°S, and on November 23 and 27 of 1983, a polynya develops as the sea-ice concentrations there fall below about 15%. Finally, as may be seen on December 1 and 13 of 1983, the Ross Sea ice field then dissipates rapidly with the area of deep encavement over the continental shelf leading the way.

Seasonal Variation in Cross-Correlation in the Three Seas

The previous section describes the detailed spatial structure of the cross-correlation of sea ice with topography within our three study areas. The discussion focuses on the

development of encavements in sea ice relative to the presence of topographic highs. In doing so, it treats conditions on a selected number of days drawn largely from the weeks covering the Austral winter and spring. Here we examine the seasonal variation in these cross-correlations by treating their temporal evolution over the entire year.

Our approach is to determine time series depicting the seasonal variation in the distribution of cross-correlation within each of the three study areas. We summarize each of these distributions using three time series, including a time series of each of the upper and the lower quartile and the median cross-correlation. The results appear in Figure 9, where each series depicts a smooth of the data obtained by interpolating a moving average of 3.

The time series for the Maud Rise region appear in the upper panel of Figure 9. The series illustrates the typical seasonal pattern for regions situated over the open ocean, being driven by the cycle of growth and dissipation undergone by the sea ice field. The gap in the time series represents missing values or indeterminant cross-correlations, which occur in Austral summer when open water covers the study area. The ice begins to grow over the deep waters of the study area sometime in April, 1983. At the same time, sea-ice concentrations are relatively low and decrease toward the edge of the ice field, which accounts for the valley of negative cross-correlations occurring in May and June of 1983. In the following months, there is an increasing trend in cross-correlation, both in level and in variability, to its winter and spring peak of positive cross-correlation. This, of course, is the season of the Maud-Rise encavement described in detail above. Finally, note that the distribution of cross-correlations remains reasonably symmetric throughout the year.

The Ross Sea time series appear in the middle panel of Figure 9. With the exception of March and April when the Ross Sea ice field begins growing, the median cross-correlation is positive in all of 1983. Moreover, the distribution of cross-correlations is one of predominantly positive cross-correlations, particularly in late fall, winter, and early spring. This is the period when the Ross Sea encavement hovers persistently above the shallow waters of the continental shelf. At other times, particularly during the summer months of 1983, the distributions are more variable and contain more negative cross-correlations, reflecting both the edge effect and the persistence of higher concentrations at some shallow sites.

Finally, the time series for the Cosmonaut Sea study area appear in the lower panel of Figure 9. From January 1983 to early May of 1983, we witness a period of strong negative cross-correlation as the developing edge of the ice field extends over the deepening waters in the study area. In the following months, there is an increasing trend in cross-correlation to its winter peak, but unlike the other study areas, the median cross-correlation here never exceeds more than about -0.2. The predominance of negative cross-correlation reflects the strong edge effect described above. On the other hand, the winter distribution of cross-correlation appears somewhat skewed to the positive direction as the percentile time series are positioned asymmetrically about the median series. As discussed in detail above, the positive extremes in cross-correlation occur in the vicinity of the Astrid Ridge, which localizes the occurrence of an encavement in the Cosmonaut Sea.

4. Discussion

The results presented here suggest a role for seabed topography in accounting for large-scale variations in Antarctic sea ice. They show quantitatively, for example, that the presence of topographic features of high elevation correlate with the occurrence of encavements in sea ice. This relationship is particularly evident with respect to the Antarctic-Pacific Ridge, the Astrid Ridge, Maud Rise, the continental shelf in the Ross and Cosmonaut Seas, as well as other high-elevation features in the seabed. An exploration of the connection between these results and those demonstrating a role for oceanographic and atmospheric effects remains in prospect.

The relationship established here is quantified in terms of the spatial cross-correlation between sea-ice concentration and ocean depth. In doing so, we implemented a statistical image-processing filter that selects for features of strong cross-correlation. After processing a year's worth of data in this way, we animated the results in what proved to be our most powerful data-analytic technique for information extraction from a time series of satellite images. The use of color graphics to well represent subranges of sea-ice variation was integral to our work. Throughout, we found the research of *Vasyutin and Tishchenko* [1989] helpful in developing the color keys used in our image processing routines. Overall, our techniques will prove valuable in many areas of environmental analysis.

We studied the structure of the spatial cross-correlation field in detail in three study areas drawn from the Weddell Sea, the Cosmonaut Sea, and the Ross Sea. This provided examples of the relationship described above. In the Weddell Sea study area for instance, we showed that Maud Rise localized the occurrence of the Maud-Rise encavement, whereas the continental shelf localized the encavement found in the Ross Sea. In each case, the encavement developed into a polynya and an embayment in the sea ice field near winter's end. The Astrid Ridge localized a similar event in the Cosmonaut Sea study area, along with a weaker continental-shelf effect. Peak periods for these strong spatial cross-correlations occurred over the Austral winter and spring.

We understand our results in terms of the role basal melting plays in the development of encavements in sea ice. We suspect that, as they encounter topographic features such

as ridges, seamounts, and the slope of the continental shelf, volumes of warmer water from deep ocean currents are directed to the surface, where they melt the ice from below. Otherwise, we cannot sustain the striking coherence found here between the topography of the seabed and the spatial variation observed in the sea ice itself. Once an encavement becomes a polynya or an embayment, of course, other factors such as katabatic winds help sustain or enlarge the area of open water.

This understanding is consistent with other studies of sea-ice processes in Antarctica. In specific, *Comiso and Gordon* [1987] explored the oceanographic conditions at the sites of the Cosmonaut and Maud-Rise polynyas as observed in 1980. They found temperature and salinity distributions characteristic of the doming of warmer, saltier deep water. In the case of Maud Rise, for example, they as well as *Gordon and Huber* [1990] speculate that convective upwelling of warmer Weddell deep water may, as part of a sequence of environmental events, induce a polynya to form by melting the sea ice from below. The role of the seamount lies in redirecting the circulating deep ocean currents toward the surface.

In the Ross Sea, *Pillsbury and Jacobs* [1985] investigated the flow of warm water from the circumpolar deep water southward across the continental shelf and into the sub-ice shelf cavity. They found that midwinter intrusions of warm water in July can raise the average temperature there from -2.19°C to -0.14°C, and they estimated that the ocean supplies enough heat to melt 150 km^3/yr of ice off the base of the Ross Ice Shelf. Their observational period covers the winter of 1983, leading us to imagine that basal melting contributed to the Ross-Sea encavement observed here. On the other hand, *MacAyeal* [1985] investigated basal melting in a numerical simulation of tidal activity in the Ross Sea. He showed that periodic tidal currents redirect barotropic circulations along topographic features such as bumps and ridges in the seabed, thereby channeling the flow of warm water needed to induce such melting. Thus, the role of the seabed lies again in redirecting the circulating currents toward the area of encavement.

It remains to investigate the role of seabed topography in determining other properties of the sea ice. For example, its role in determining rates of growth and dissipation as well

as the final shape of the ice field need to be better understood. Also, we infer from our results that some of the first-order or large-scale variation in sea ice can be modeled in terms of ocean depth. We therefore propose to fit such a model to these data and analyze the remaining fluctuations for both their natural variation and their covariation with other environmental processes.

Acknowledgements. The authors were partially supported by National Aeronautics and Space Administration Grant 3488-OP-629. We thank J. Comiso, A. Gordon, and S. Jacobs for providing both the data and fruitful discussion leading to this research.

References

[1] Becker, R. A., J. M. Chambers, and A. R. Wilks, *The New S Language, A Programming Environment for Data Analysis and Graphics*, Wadsworth and Brooks/Cole, Pacific Grove, CA, 1988.

[2] Cavalieri, D. J. and S. Martin, A passive microwave study of polynyas along the Antarctic Wilkes Land Coast, in *Oceanology of the Antarctic Continental Shelf*, Antarctic Research Series, Vol. 43, 227 252, edited by S. Jacobs, American Geophysical Union, Washington, D.C., 1985.

[3] Comiso, J. C. and H. J. Zwally, Polar microwave brightness temperatures from Nimbus-7 SMMR: Time series of daily and monthly maps from 1978-1987, NASA Technical Memorandum 1223, National Aeronautics and Space Administration, Laboratory for Oceans, Goddard Space Flight Center, Greenbelt, MO 20771, 1989.

[4] Comiso, J. C. and A. L. Gordon, Recurring polynyas over the Cosmonaut Sea and the Maud Rise, *J. Geophys. Res.*, 92 (C3), 2819 2833, 1987.

[5] Gordon, A. L. and B. A. Huber, Southern Ocean winter mixed layer, in press *J. Geophys. Res.*, 1990.

[6] Kurtz, D. D. and D. H. Bromwich, A recurring, atmospherically forced polynya in Terra Nova Bay, in *Oceanology of the Antarctic Continental Shelf*, Antarctic Research Series, Vol. 43, 177 202, edited by S. Jacobs, American Geophysical Union, Washington, D.C., 1985.

[7] MacAyeal, D. R., Tidal rectification below the Ross Ice Shelf, Antarctica, in *Oceanology of the Antarctic Continental Shelf*, Antarctic Research Series, Vol. 43, 109 132, edited by S. Jacobs, American Geophysical Union, Washington, D.C., 1985.

[8] Pillsbury, R. D. and S. S. Jacobs, Preliminary observations from long-term current meter mooring near the Ross Ice Shelf, Antarctica, in *Oceanology of the*

Antarctic Continental Shelf, Antarctic Research Series, Vol. 43, 87 108, edited by S. Jacobs, American Geophysical Union, Washington, D.C., 1985.

[9] VASYUTIN, V. V. AND A. A. TISHCHENKO, Space Coloristics, *Scientific American*, Vol. 261, July 1989.

[10] ZWALLY, H. J., J. C. COMISO, AND A. L. GORDON, Antarctic offshore leads and polynyas and oceanographic effects, in *Oceanology of the Antarctic Continental Shelf*, Antarctic Research Series, Vol. 43, 203 226, edited by S. Jacobs, American Geophysical Union, Washington, D.C., 1985.

FIGURE CAPTIONS

Fig. 1. Sea-ice images depicting the Antarctic sea ice field at selected days in 1983. The color key appears in Exhibit 1. Moving from left to right and top to bottom, the images depict conditions at days chosen from early March, April, July, mid and late August, early October, mid November and December, and end of December. At mid December, we see both the Maud Rise and Ross Sea polynyas.

Fig. 2. Bathymetry image depicting the seabed topography about Antarctica. The color key appears in Exhibit 1.

Fig. 3. Scatterplot of sea-ice concentration against ocean depth at the scale of the entire ice field in each of the Austral seasons. The absence of simple linear structure here suggests the need to search for such structure at smaller spatial scales.

Fig. 4. Cross-correlation images depicting local patterns of spatial cross-correlation between sea-ice concentration and ocean depth. The images were derived from those of Figure 1, and the color key appears in Exhibit 1. They quantify a role for seabed topography in accounting for variations in sea ice. Several examples are treated in the text, including the features of positive cross-correlation detected in the Ross Sea and near Maud Rise.

Fig. 5. Bathymetric contours depicting the seabed topography in the study area in each of the Weddell Sea, the Cosmonaut Sea, and the Ross Sea. These areas cover, for example, the sites of the 1980 Maud Rise and Cosmonaut polynyas as well as the site of the Ross-Sea encavement observed here.

Fig. 6. Time series of sea-ice concentration and cross-correlation fields in the Weddell Sea study area at selected days in 1983. They depict, for example, the development of the Maud-Rise encavement in relation to the topography around Maud Rise.

Fig. 7. Time series of sea-ice concentration and cross-correlation fields in the Cosmonaut Sea study area at selected days in 1983. They depict, for example, the development of an encavement in relation to the topography along the Astrid Ridge.

Fig. 8. Time series of sea-ice concentration and cross-correlation fields in the Ross Sea study area at selected days in 1983. They depict, for example, the development of the Ross-Sea encavement in relation to the topography of the continental shelf in the Ross Sea.

Fig. 9. Time series depicting the seasonal variation of the spatial cross-correlation between sea-ice concentration and ocean depth in each of the Weddell Sea, Ross Sea, and Cosmonaut Sea study areas. In each case, there are three time series giving the median, upper quartile, and lower quartile drawn from the distribution of cross-correlations within the study area. Gaps indicate missing values or indeterminate correlations as occurs in the absence of sea ice.

Exhibits

Exhibit 1. Color keys showing the range of data values and corresponding color scale for the images of Figures 1, 2, and 4.

Table 1 - Longitude-Latitude Pairs
at the Four Corners of the Study Areas

Weddell Sea	Cosmonaut Sea	Ross Sea
18°W, 58°S	12°E, 70°S	218°E, 75°S
23°W, 65°S	23°E, 74°S	205°E, 67°S
6°E, 58°S	35°E, 56°S	172°E, 78°S
8°E, 66°S	54°E, 65°S	175°E, 69°S

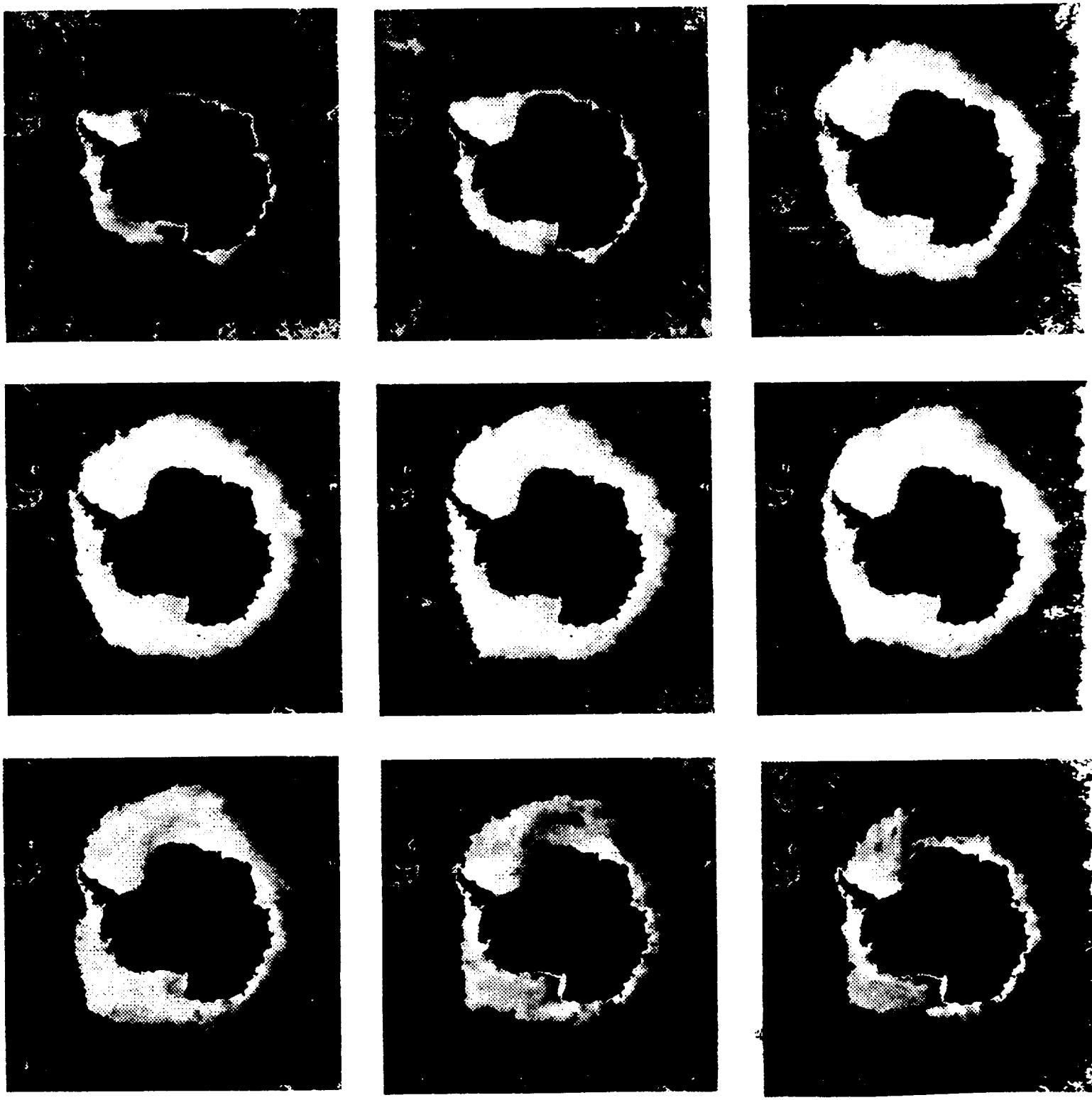

Figure 1

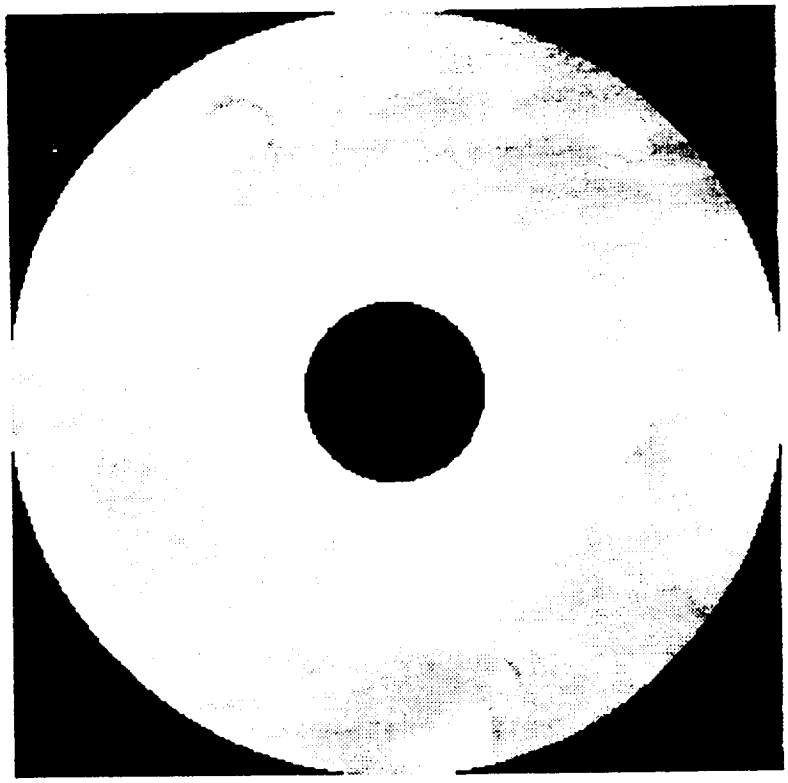

Figure 2

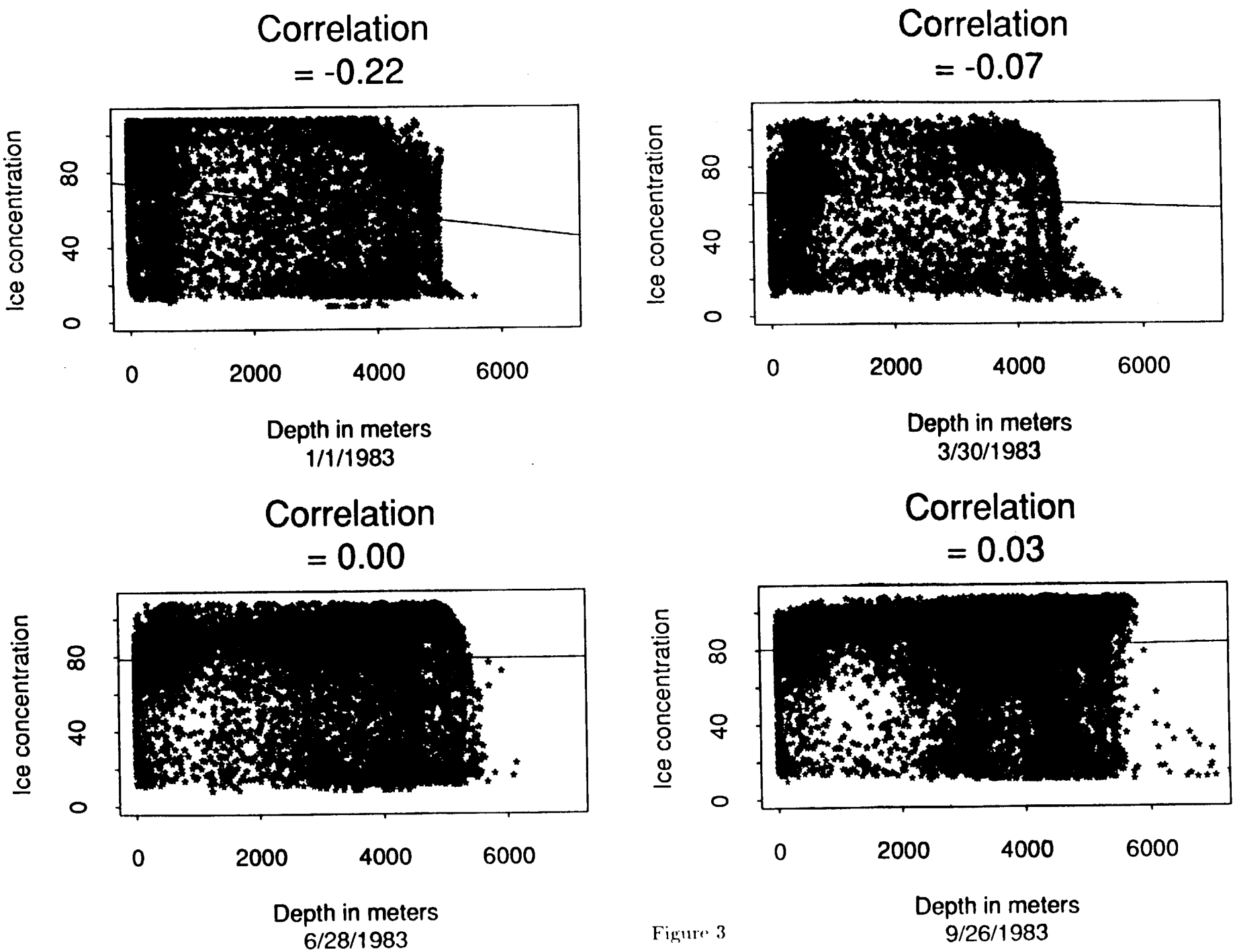
Correlation
= -0.22
Ice concentration
0
40
80
0
2000
4000
6000
Depth in meters
1/1/1983
Correlation
= -0.07
Ice concentration
0
40
80
0
2000
4000
6000
Depth in meters
3/30/1983
Correlation
= 0.00
Ice concentration
0
40
80
0
2000
4000
6000
Depth in meters
6/28/1983
Correlation
= 0.03
Ice concentration
0
40
80
0
2000
4000
6000
Depth in meters
9/26/1983

Figure 3

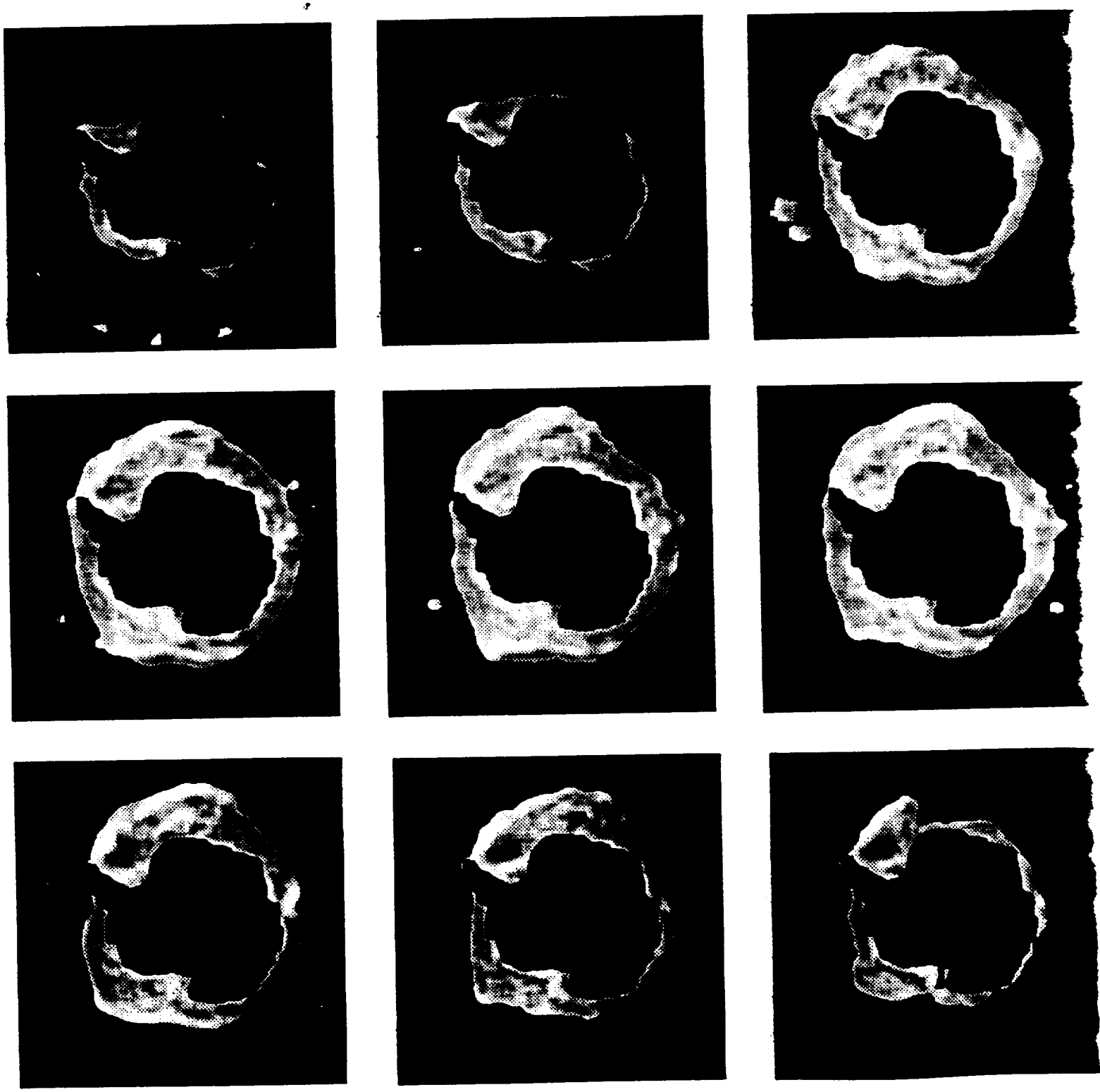

Figure 4

Bathymetry -- Depth in Meters

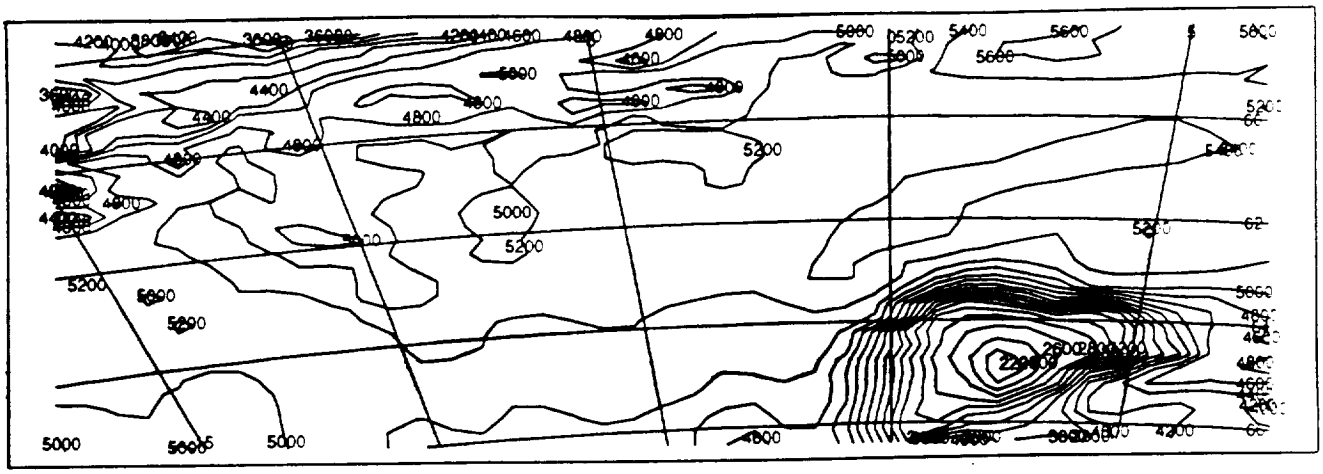

Latitude

Longitude
Weddell Sea

Bathymetry -- Depth in Meters

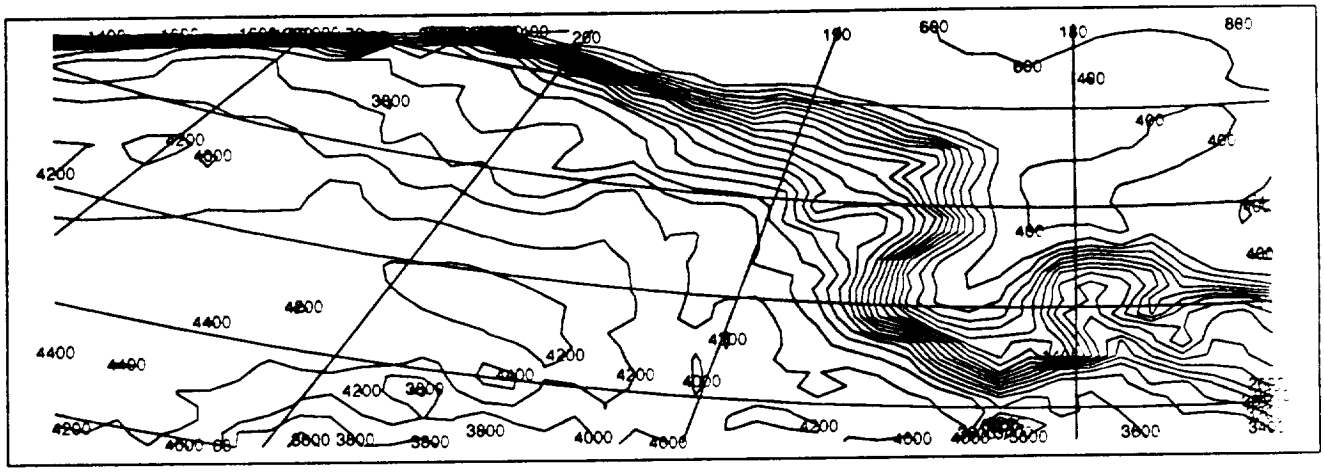

Latitude

Longitude
Ross Sea

Bathymetry -- Depth in Meters

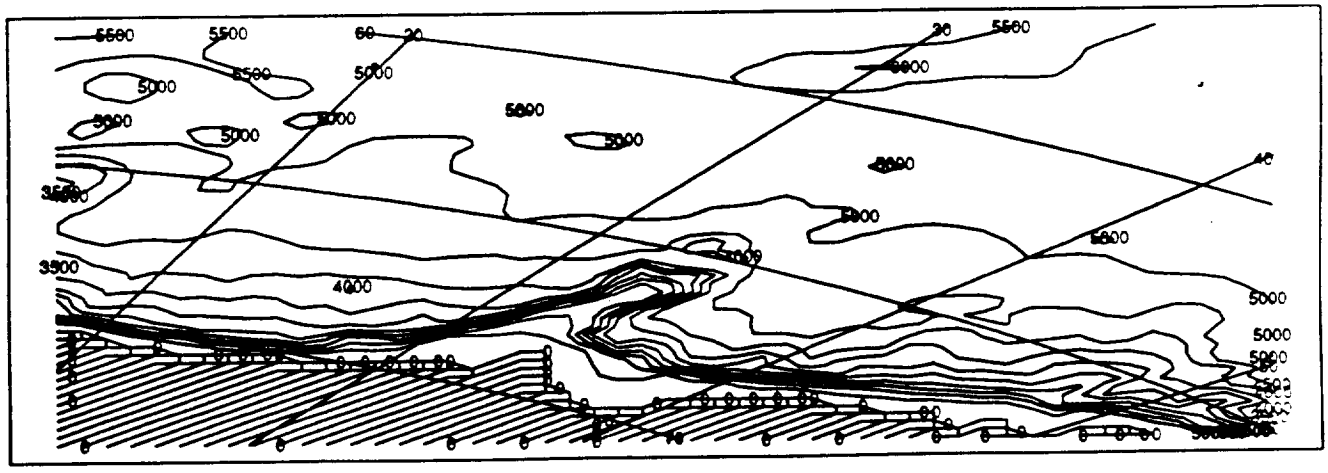

Latitude

Longitude
Cosmonaut Sea

Figure 5

Ice Concentrations

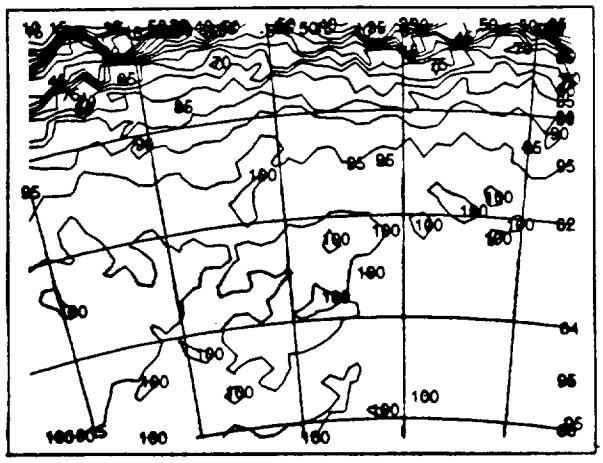

Latitude

Longitude
Weddell Sea 7/22/1983

Local Correlations

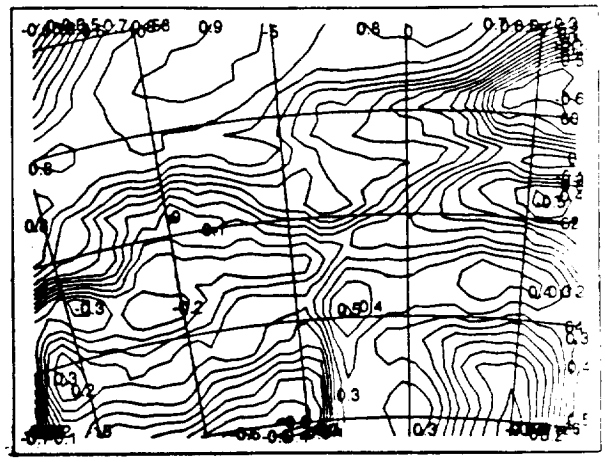

Latitude

Longitude
Weddell Sea 7/22/1983

Ice Concentrations

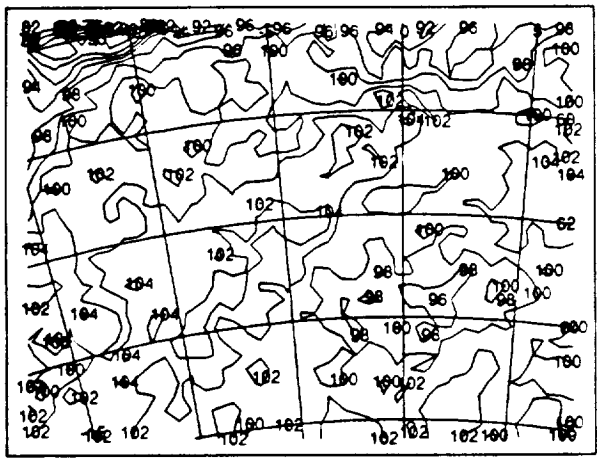

Latitude

Longitude
Weddell Sea 9/4/1983

Local Correlations

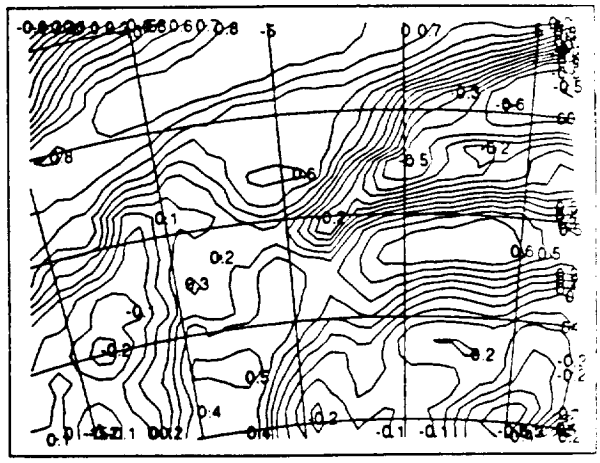

Latitude

Longitude
Weddell Sea 9/4/1983

Ice Concentrations

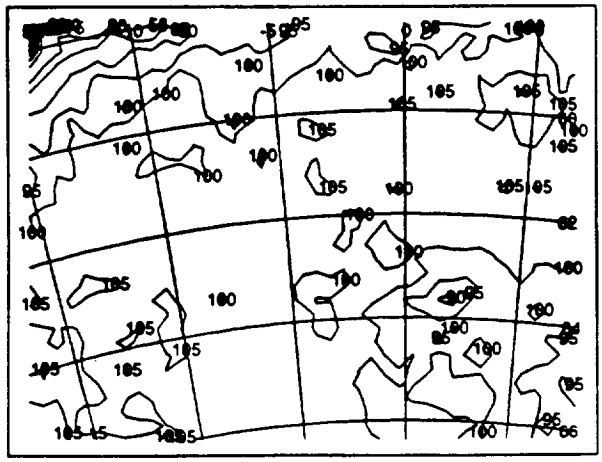

Latitude

Longitude
Weddell Sea 9/20/1983

Local Correlations

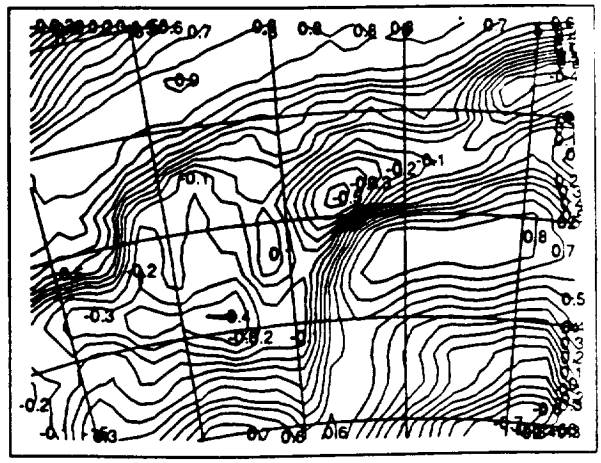

Latitude

Longitude
Weddell Sea 9/20/1983

Figure 6.a

Ice Concentrations

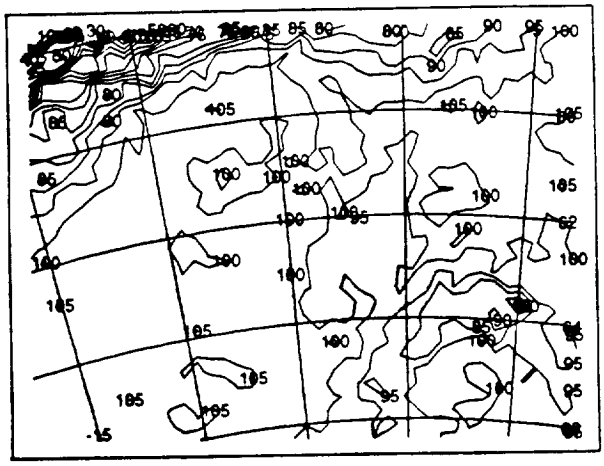

Latitude

Longitude
Weddell Sea 10/2/1983

Local Correlations

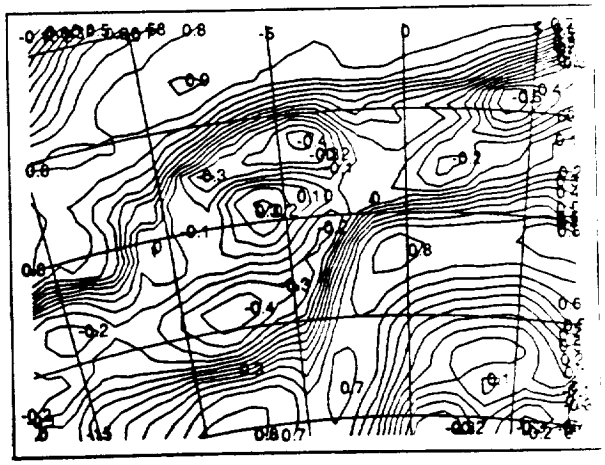

Latitude

Longitude
Weddell Sea 10/2/1983

Ice Concentrations

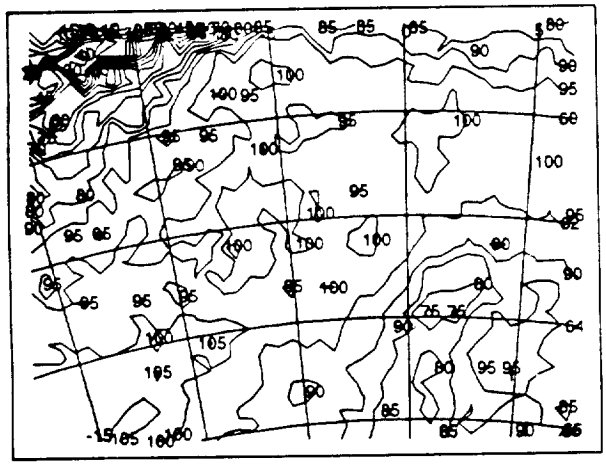

Latitude

Longitude
Weddell Sea 10/26/1983

Local Correlations

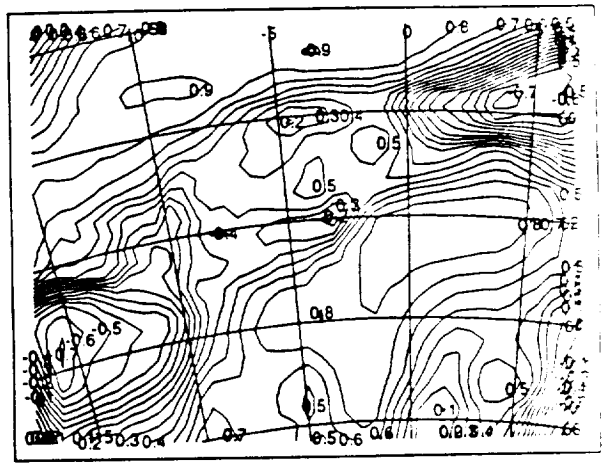

Latitude

Longitude
Weddell Sea 10/26/1983

Ice Concentrations

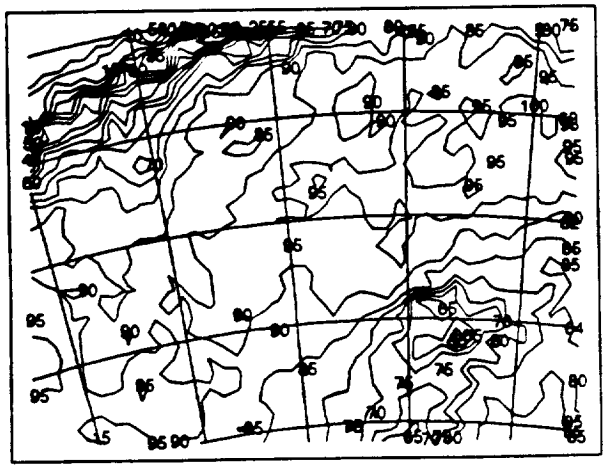

Latitude

Longitude
Weddell Sea 11/3/1983

Local Correlations

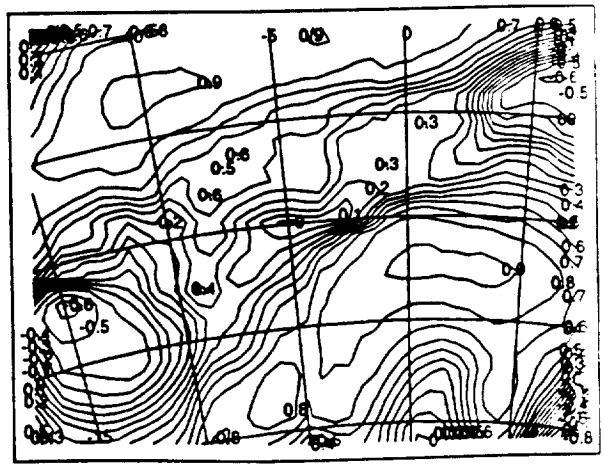

Latitude

Longitude
Weddell Sea 11/3/1983

Figure 6.b

Ice Concentrations

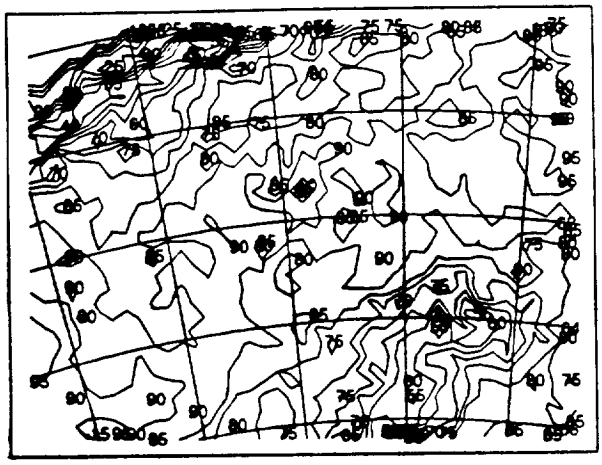

Latitude

Longitude
Weddell Sea 11/7/1983

Local Correlations

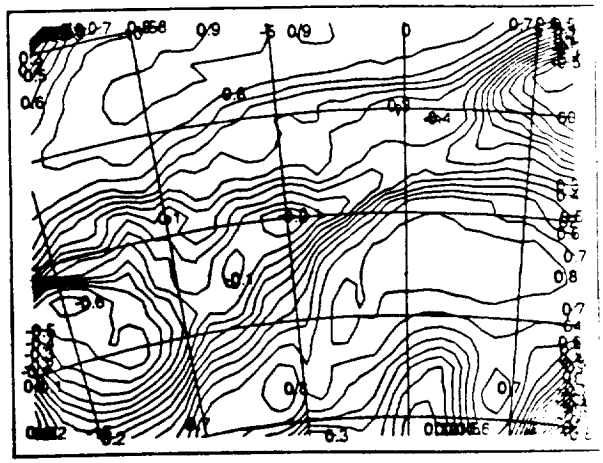

Latitude

Longitude
Weddell Sea 11/7/1983

Ice Concentrations

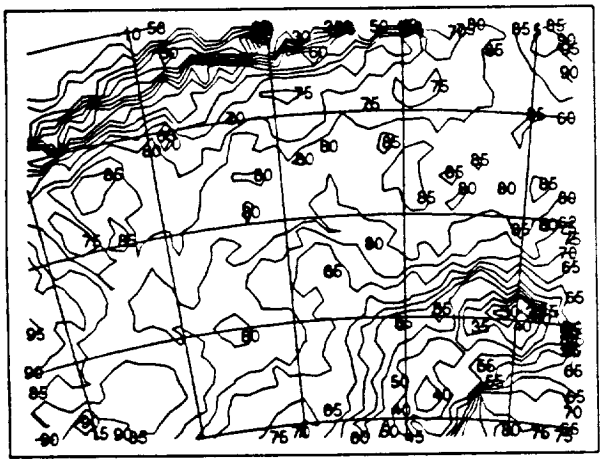

Latitude

Longitude
Weddell Sea 11/13/1983

Local Correlations

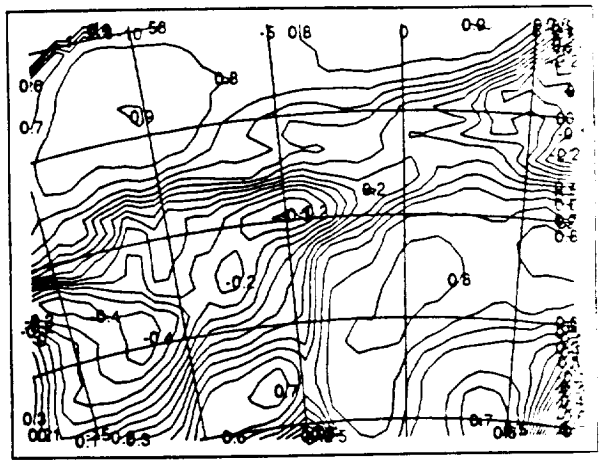

Latitude

Longitude
Weddell Sea 11/13/1983

Ice Concentrations

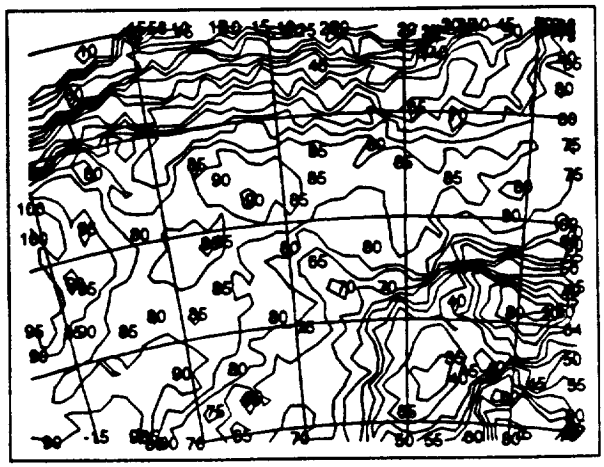

Latitude

Longitude
Weddell Sea 11/19/1983

Local Correlations

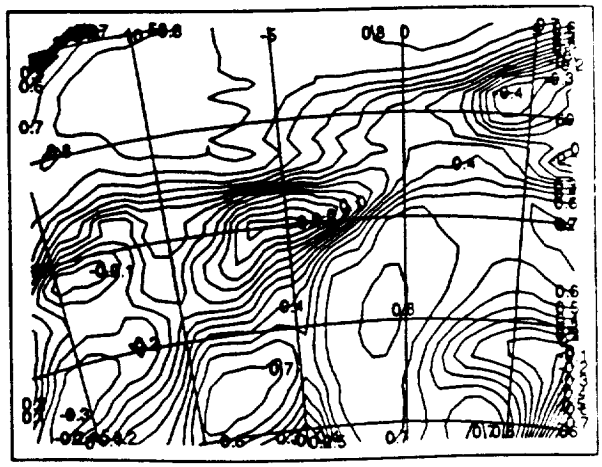

Latitude

Longitude
Weddell Sea 11/19/1983

Figure 6.c

Ice Concentrations

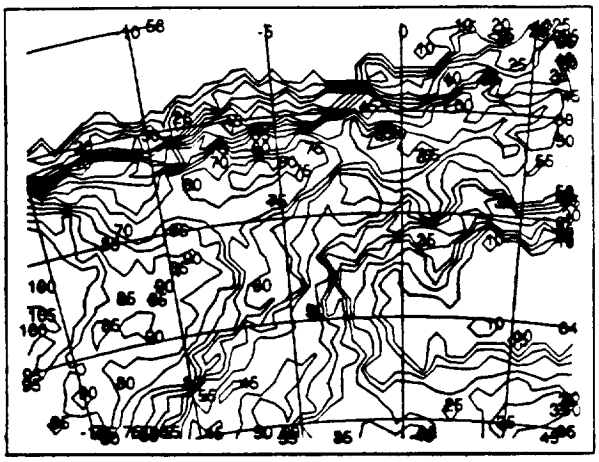

Latitude

Longitude
Weddell Sea 12/1/1983

Local Correlations

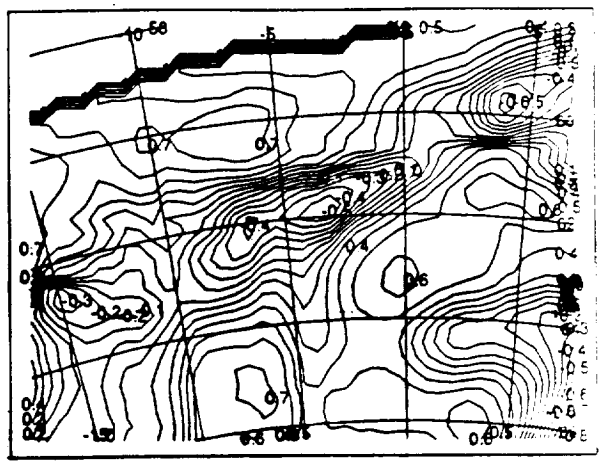

Latitude

Longitude
Weddell Sea 12/1/1983

Ice Concentrations

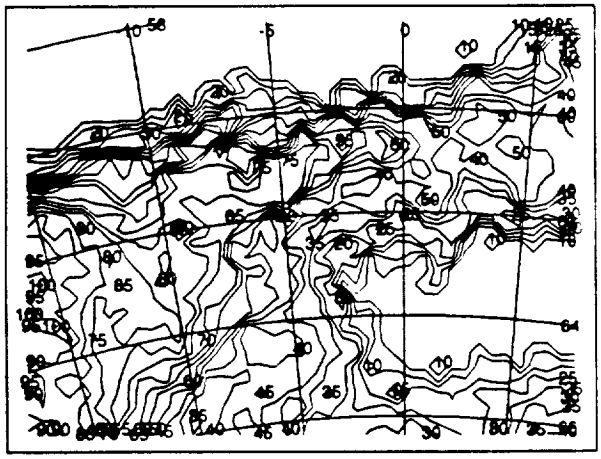

Latitude

Longitude
Weddell Sea 12/3/1983

Local Correlations

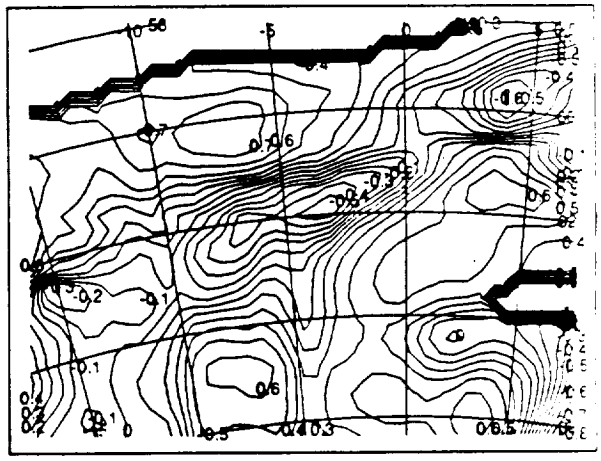

Latitude

Longitude
Weddell Sea 12/3/1983

Ice Concentrations

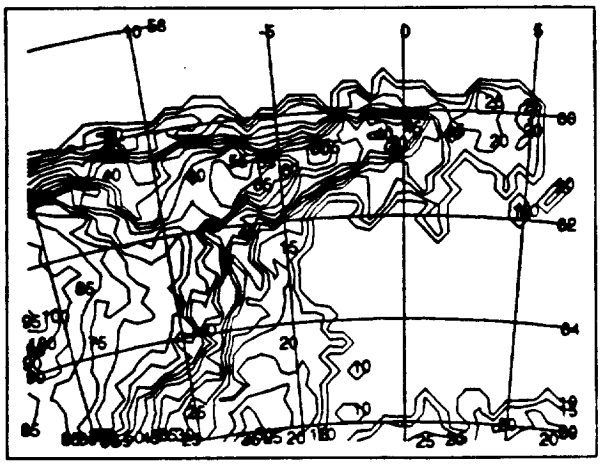

Latitude

Longitude
Weddell Sea 12/7/1983

Local Correlations

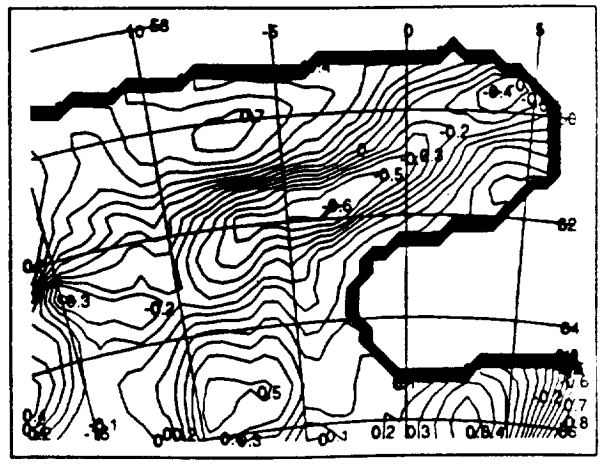

Latitude

Longitude
Weddell Sea 12/7/1983

Figure 6.d

Ice Concentrations

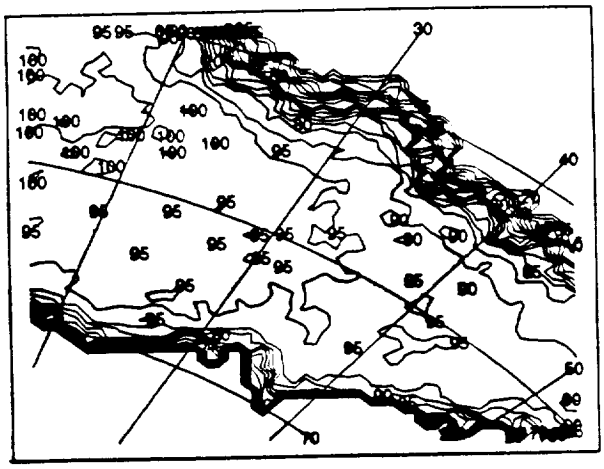

Local Correlations

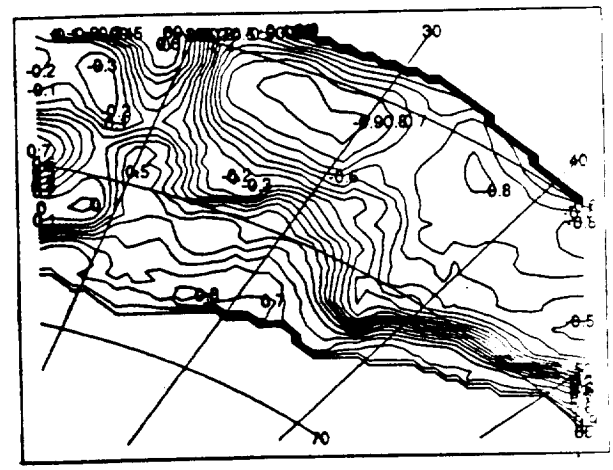

Ice Concentrations

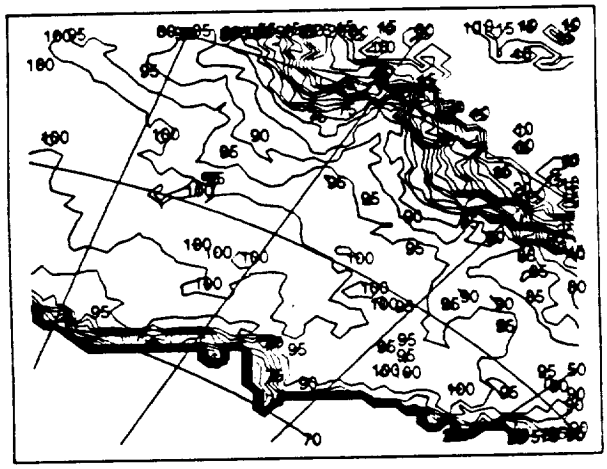

Local Correlations

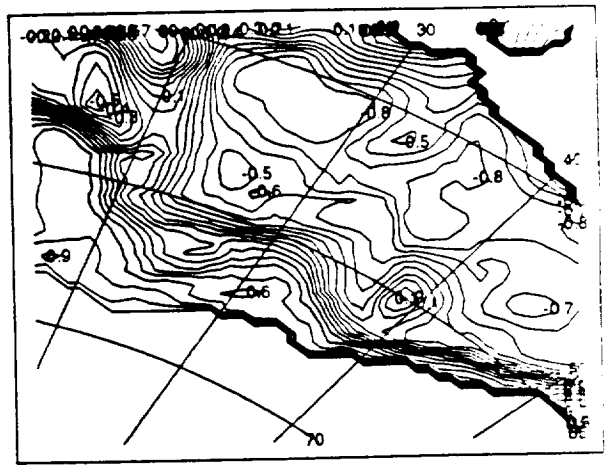

Ice Concentrations

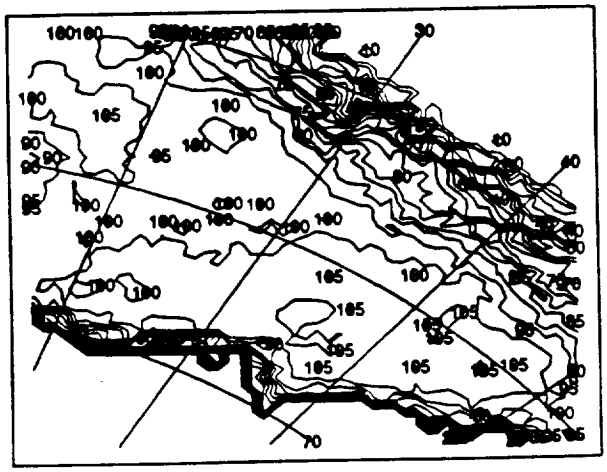

Local Correlations

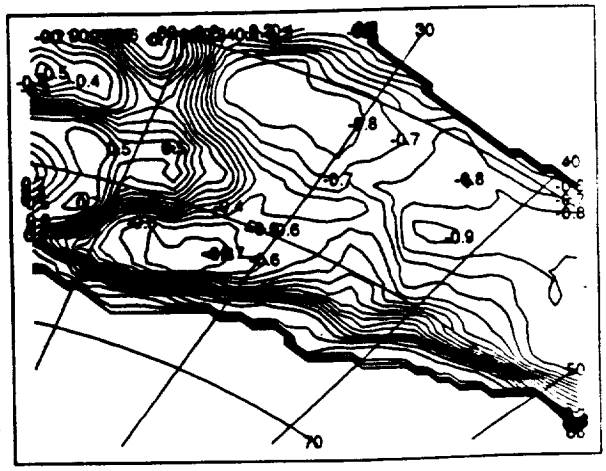

Figure 7.a

Ice Concentrations

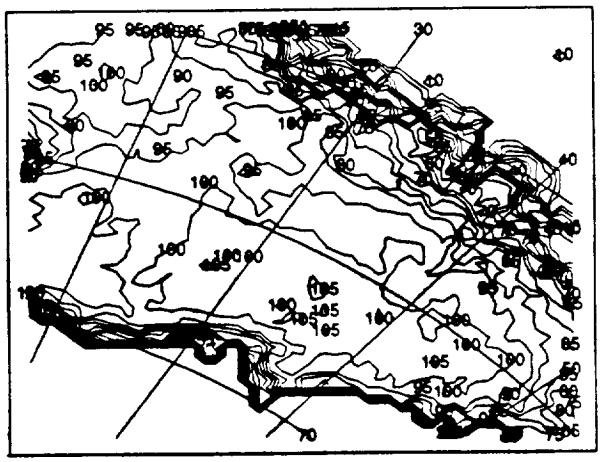

Latitude

Longitude
Cosmonaut Sea 11/5/1983

Local Correlations

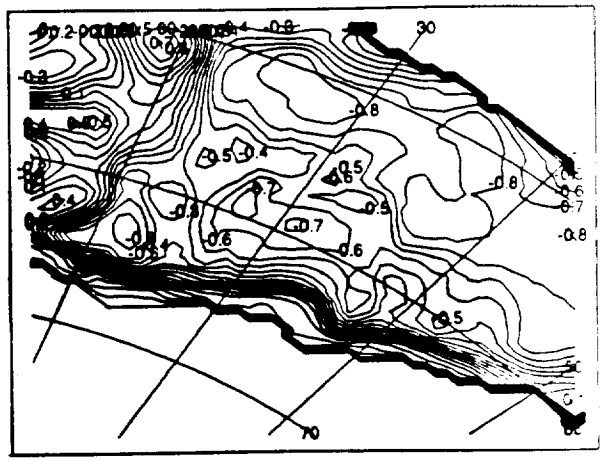

Latitude

Longitude
Cosmonaut Sea 11/5/1983

Ice Concentrations

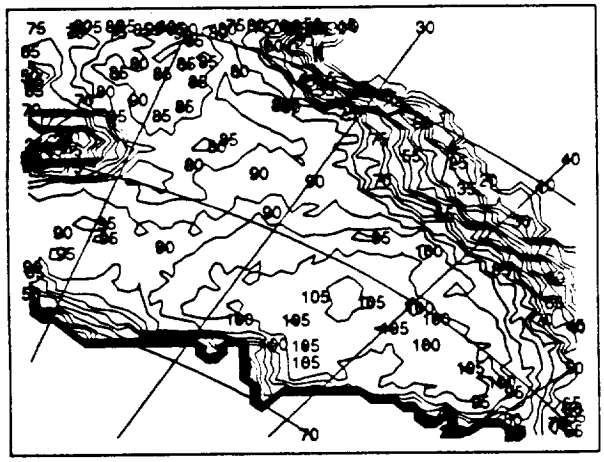

Latitude

Longitude
Cosmonaut Sea 11/17/1983

Local Correlations

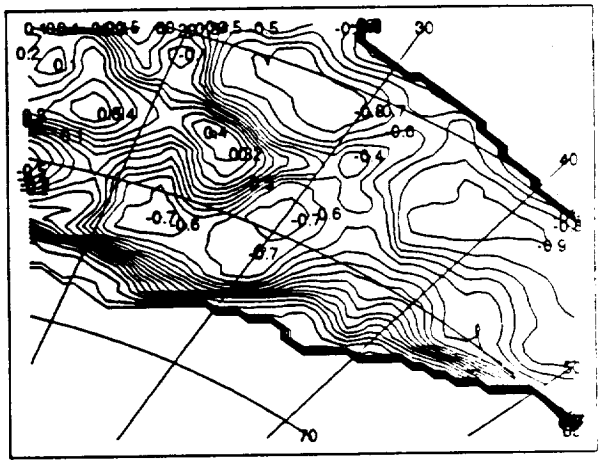

Latitude

Longitude
Cosmonaut Sea 11/17/1983

Ice Concentrations

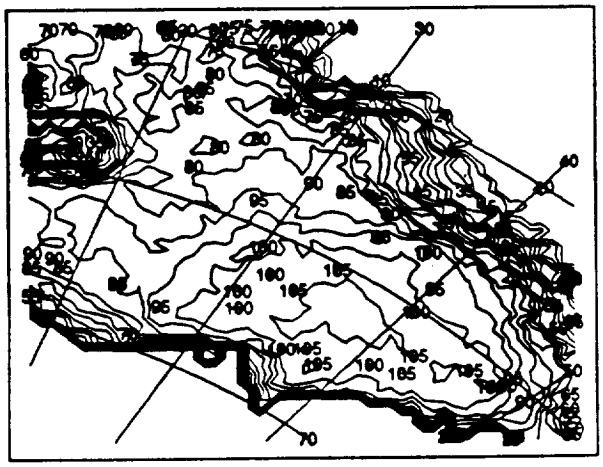

Latitude

Longitude
Cosmonaut Sea 11/19/1983

Local Correlations

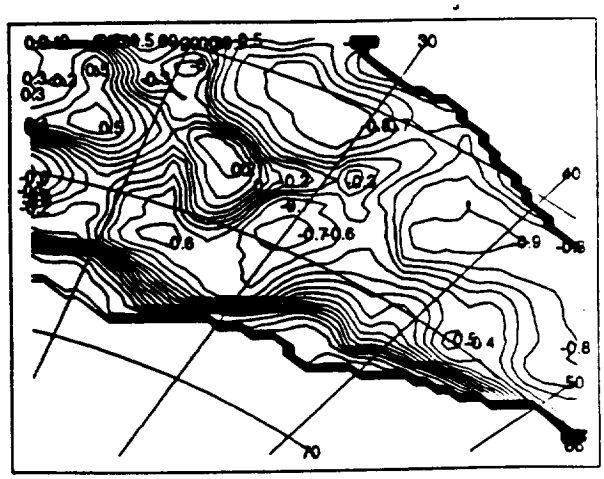

Latitude

Longitude
Cosmonaut Sea 11/19/1983

Figure 7.b

Ice Concentrations

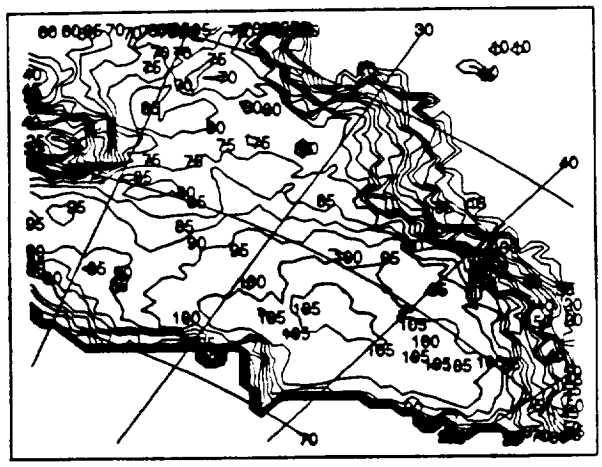

Latitude

Longitude
Cosmonaut Sea 11/23/1983

Local Correlations

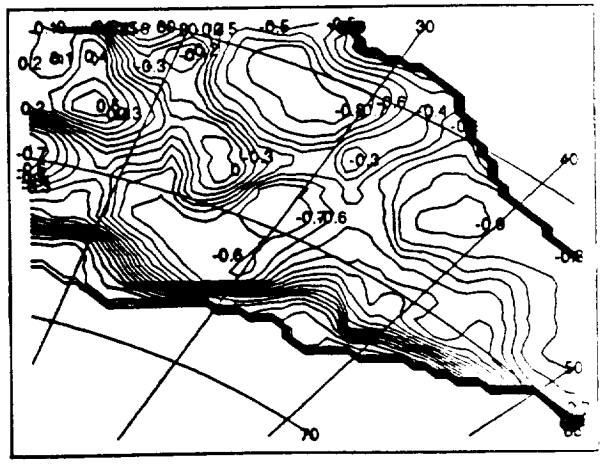

Latitude

Longitude
Cosmonaut Sea 11/23/1983

Ice Concentrations

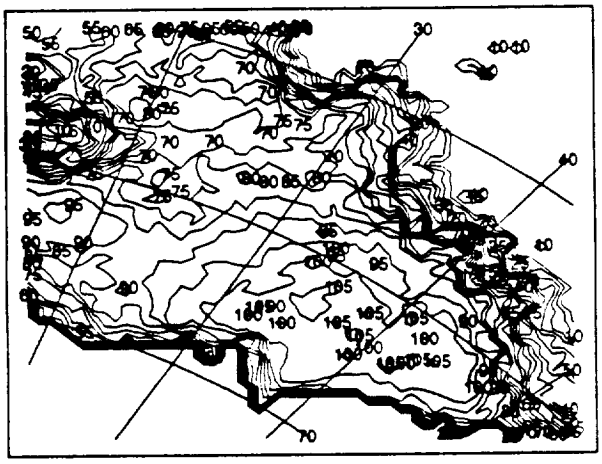

Latitude

Longitude
Cosmonaut Sea 11/25/1983

Local Correlations

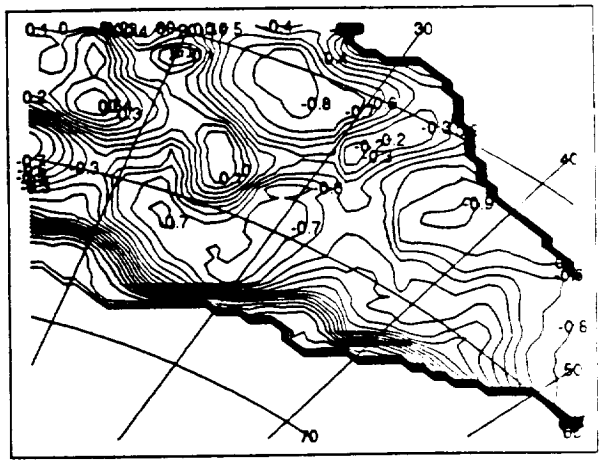

Latitude

Longitude
Cosmonaut Sea 11/25/1983

Ice Concentrations

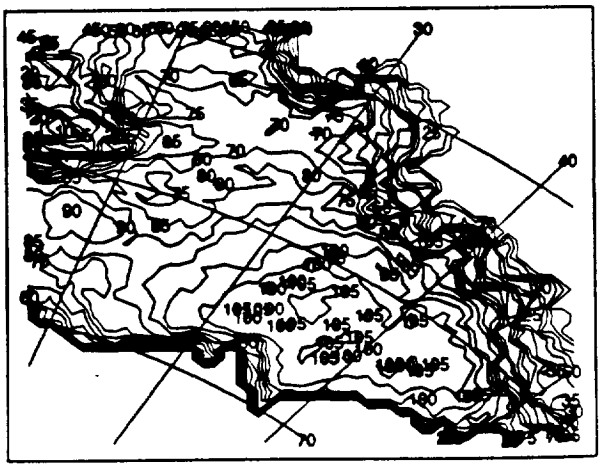

Latitude

Longitude
Cosmonaut Sea 11/27/1983

Local Correlations

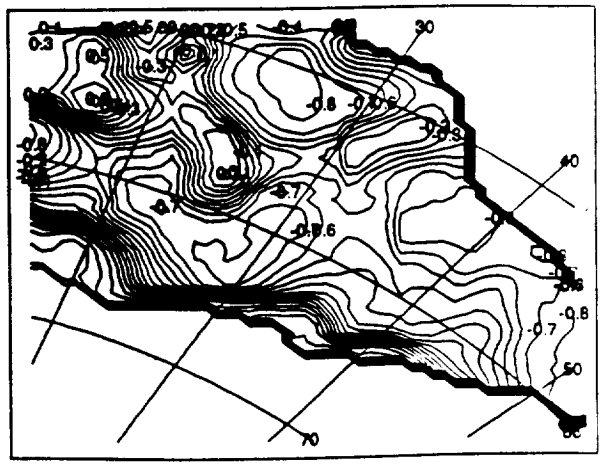

Latitude

Longitude
Cosmonaut Sea 11/27/1983

Figure 7.c

Ice Concentrations

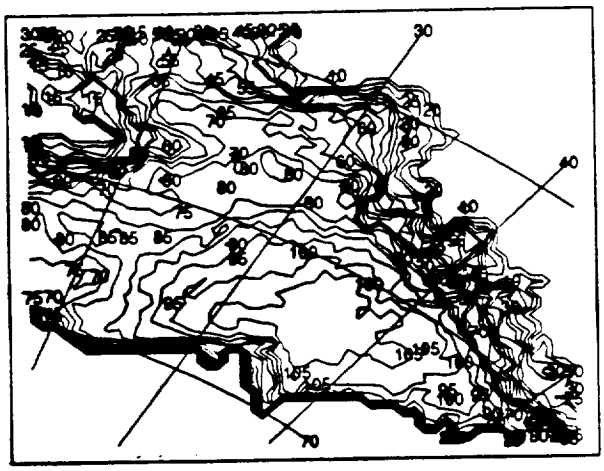

Latitude

Longitude
Cosmonaut Sea 12/1/1983

Local Correlations

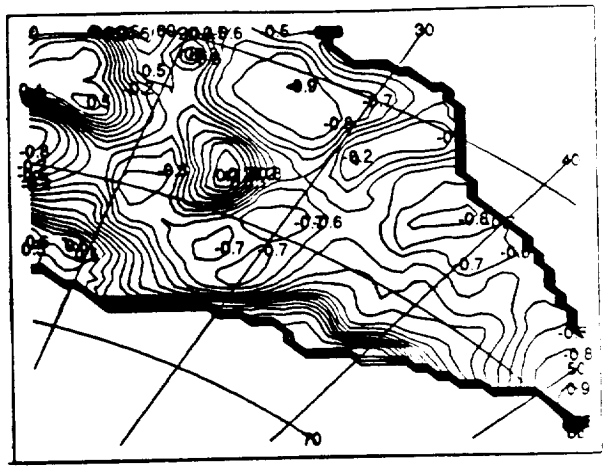

Latitude

Longitude
Cosmonaut Sea 12/1/1983

Ice Concentrations

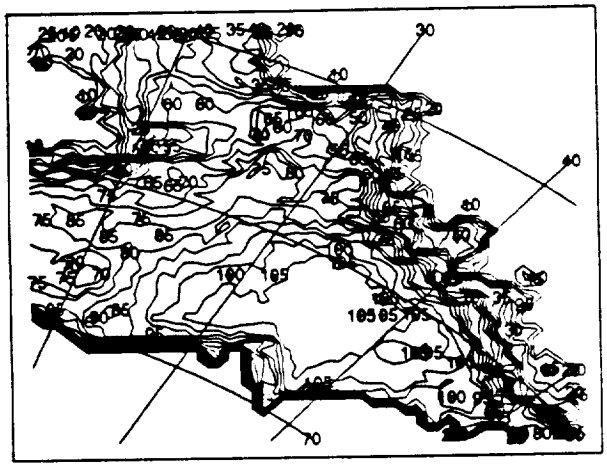

Latitude

Longitude
Cosmonaut Sea 12/3/1983

Local Correlations

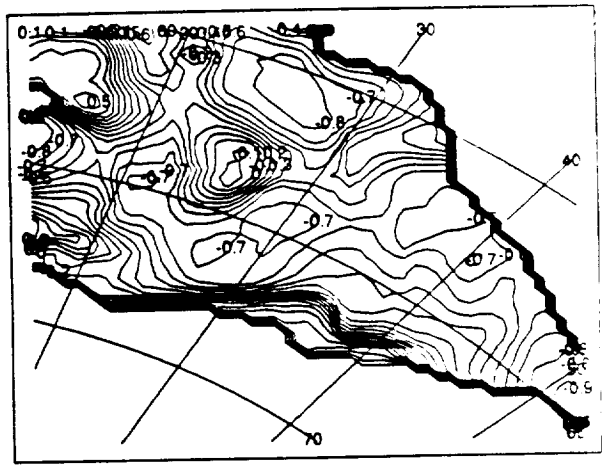

Latitude

Longitude
Cosmonaut Sea 12/3/1983

Ice Concentrations

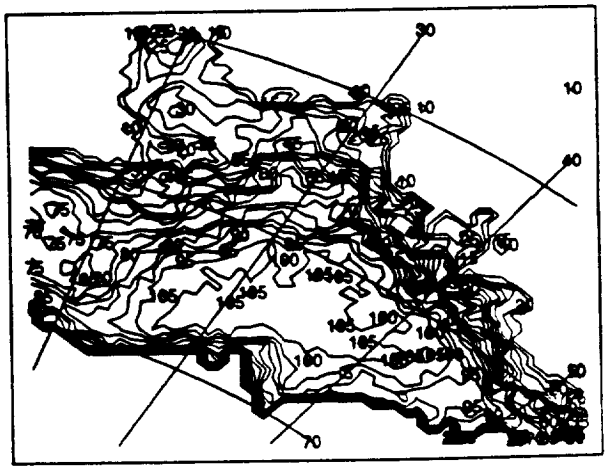

Latitude

Longitude
Cosmonaut Sea 12/7/1983

Local Correlations

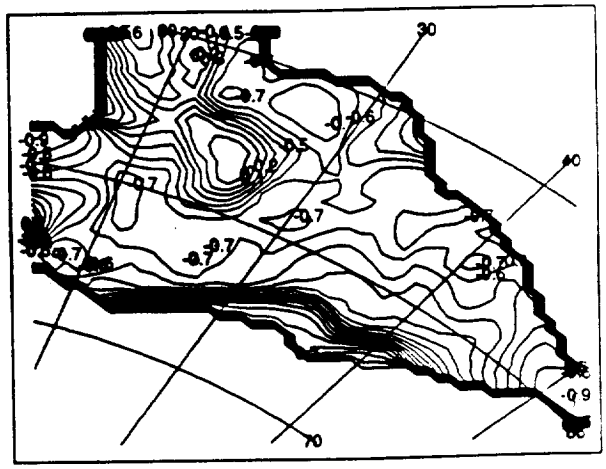

Latitude

Longitude
Cosmonaut Sea 12/7/1983

Figure 7.d

Ice Concentrations

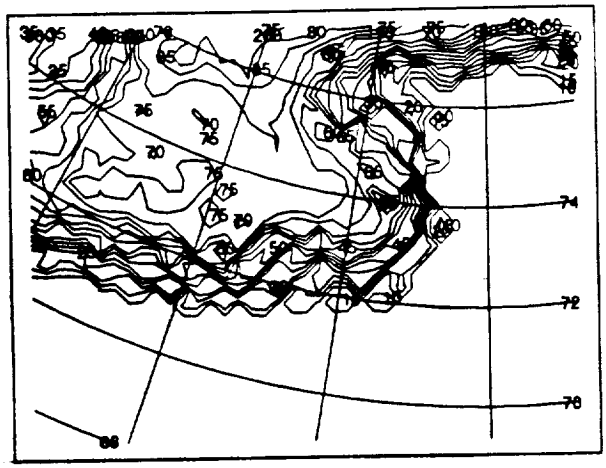

Local Correlations

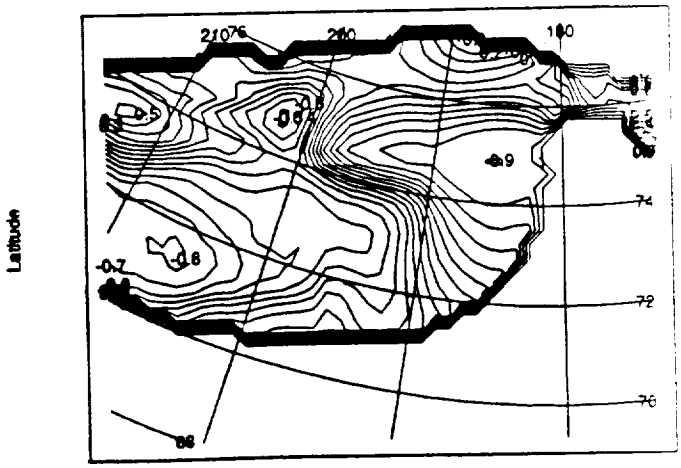

Ice Concentrations

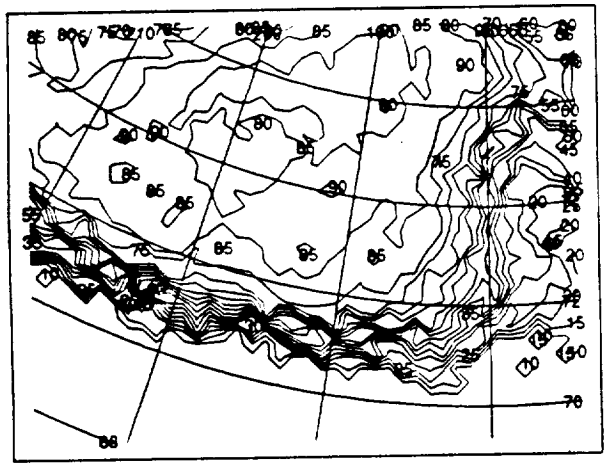

Local Correlations

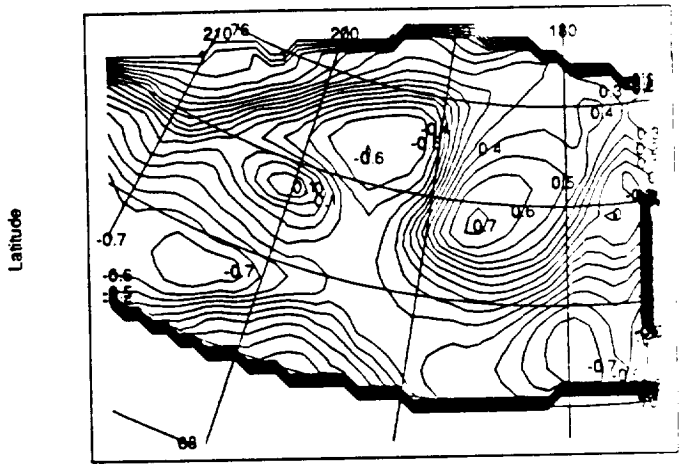

Ice Concentrations

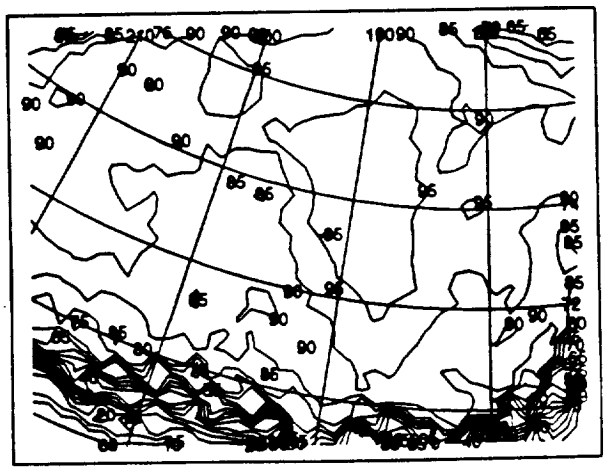

Local Correlations

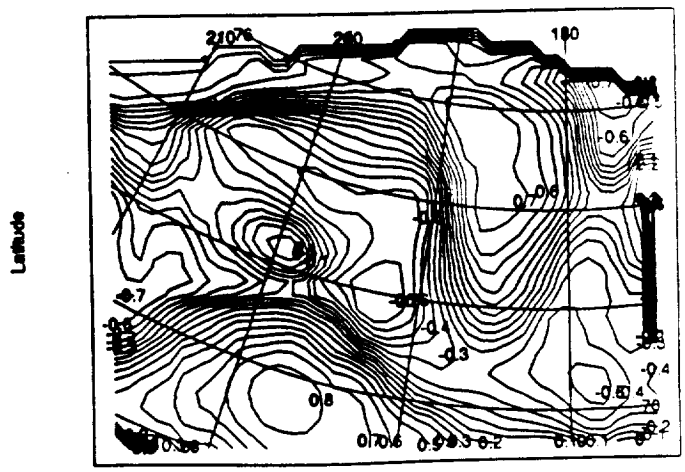

Figure 8.a

Ice Concentrations

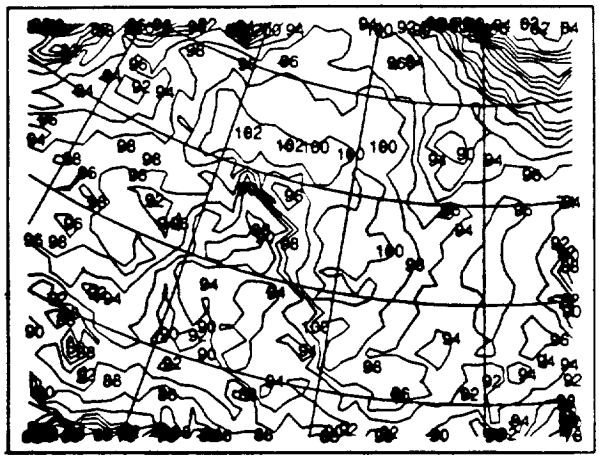

Latitude

Longitude
Ross Sea 4/27/1983

Local Correlations

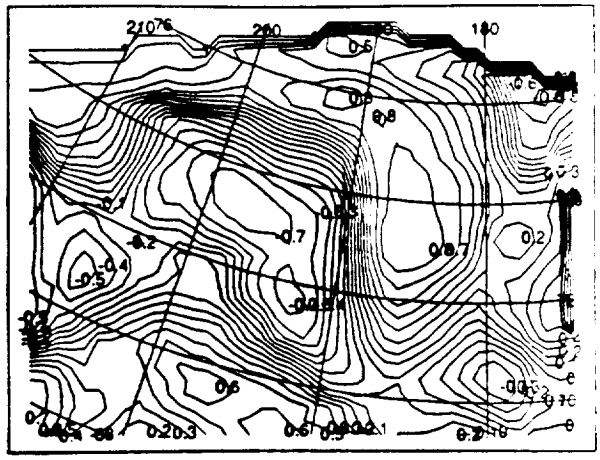

Latitude

Longitude
Ross Sea 4/27/1983

Ice Concentrations

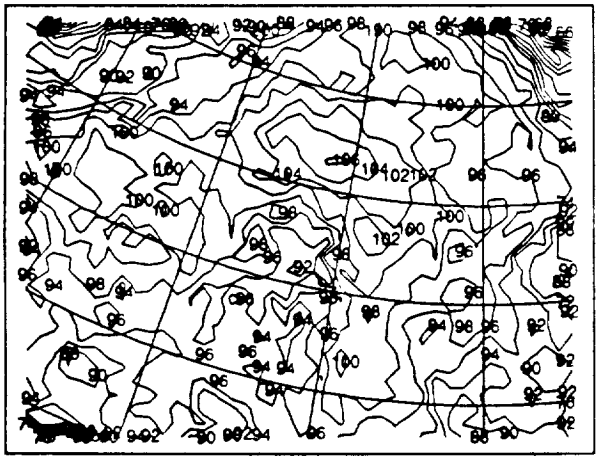

Latitude

Longitude
Ross Sea 5/11/1983

Local Correlations

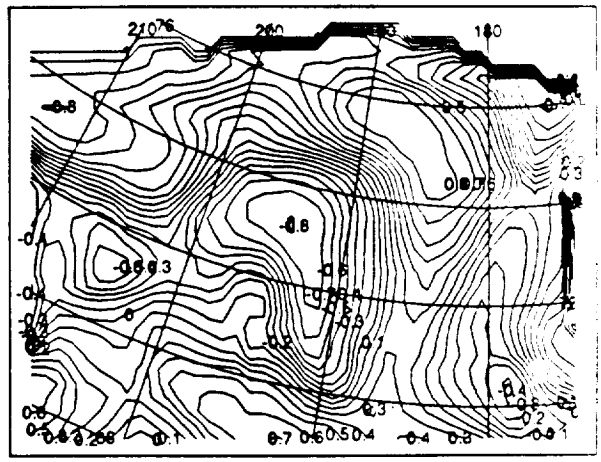

Latitude

Longitude
Ross Sea 5/11/1983

Ice Concentrations

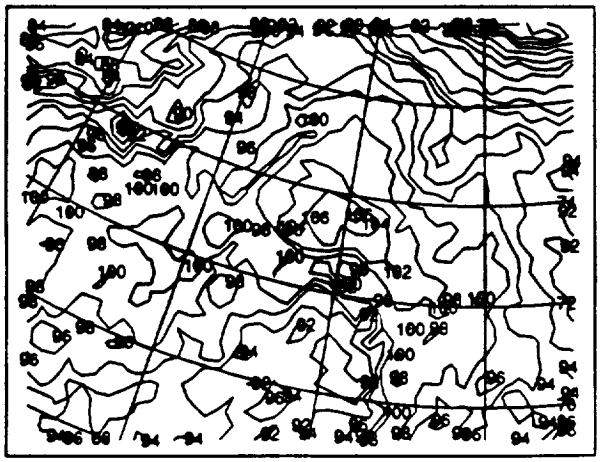

Latitude

Longitude
Ross Sea 6/6/1983

Local Correlations

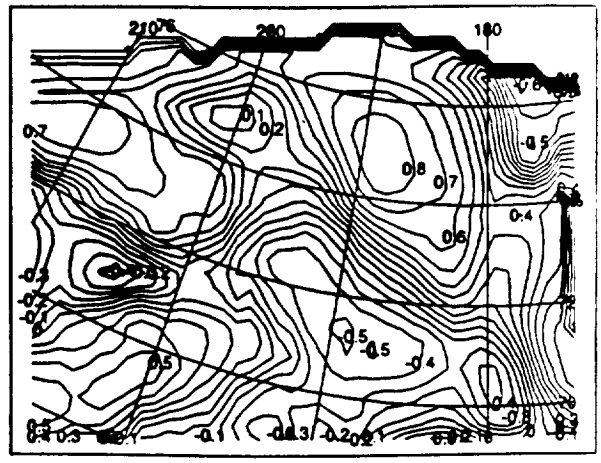

Latitude

Longitude
Ross Sea 6/6/1983

Figure 8.b

Ice Concentrations

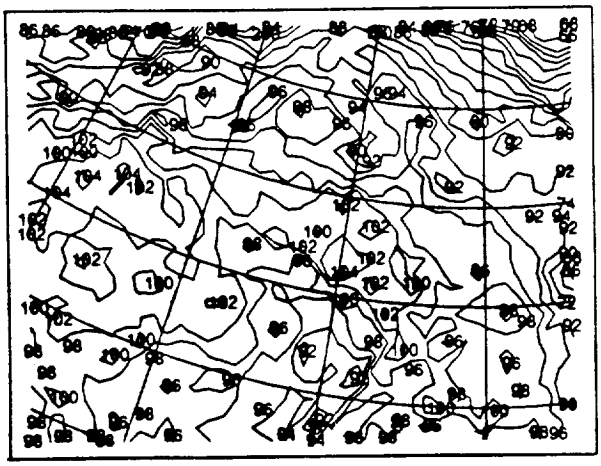

Latitude

Longitude
Ross Sea 6/22/1983

Local Correlations

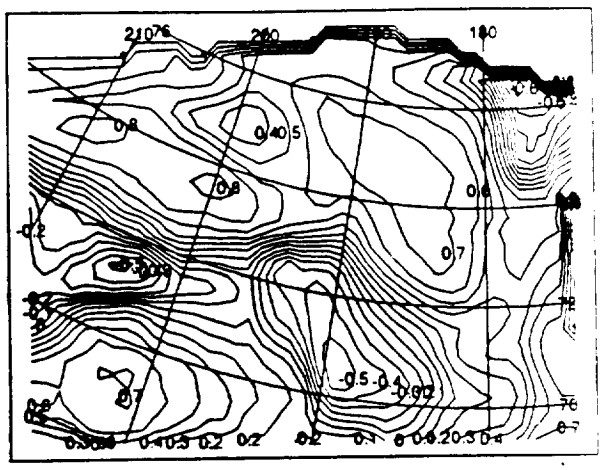

Latitude

Longitude
Ross Sea 6/22/1983

Ice Concentrations

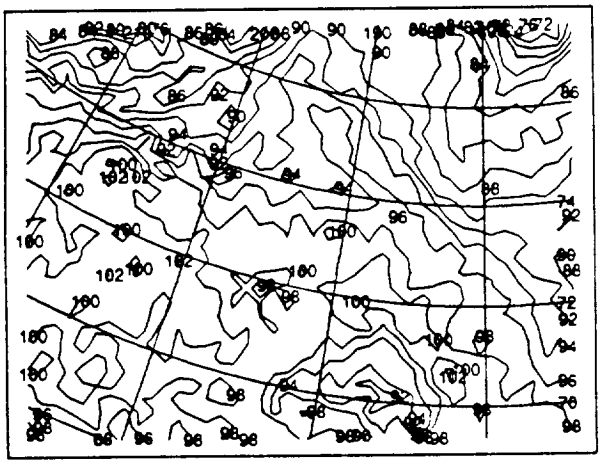

Latitude

Longitude
Ross Sea 7/6/1983

Local Correlations

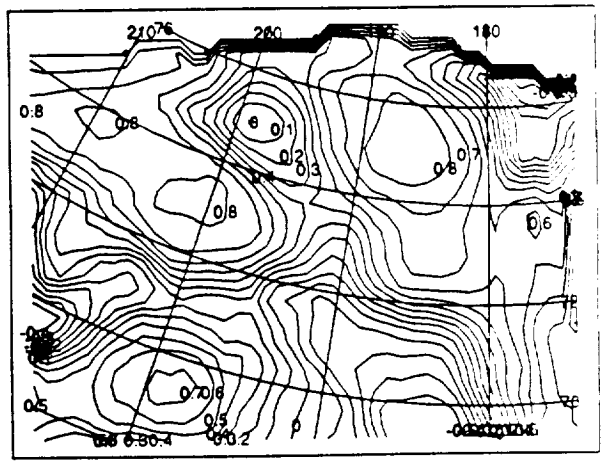

Latitude

Longitude
Ross Sea 7/6/1983

Ice Concentrations

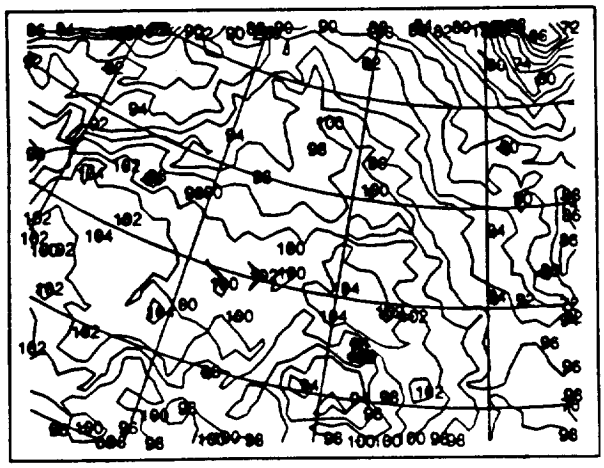

Latitude

Longitude
Ross Sea 7/22/1983

Local Correlations

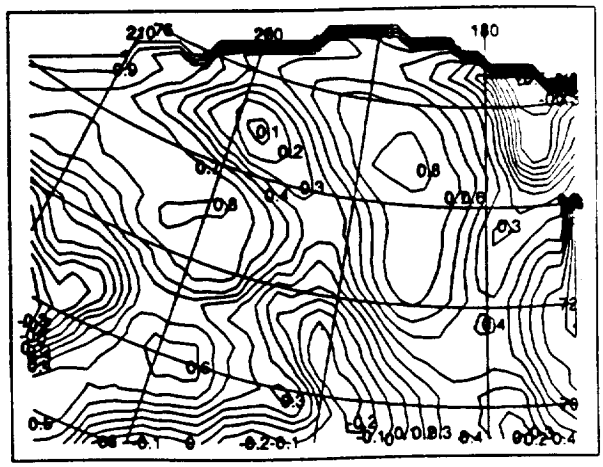

Latitude

Longitude
Ross Sea 7/22/1983

Figure 8.c

Ice Concentrations

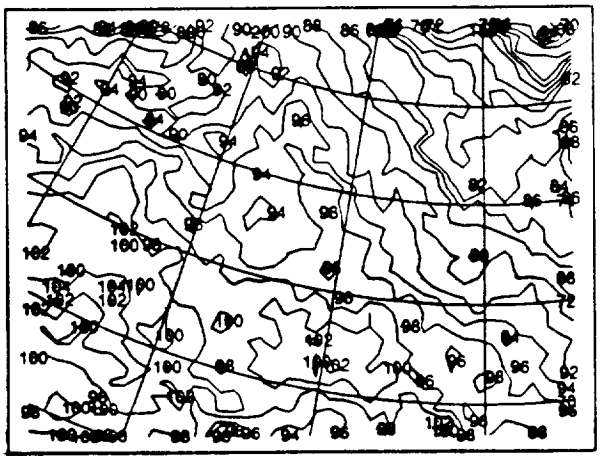

Latitude

Longitude
Ross Sea 8/15/1983

Local Correlations

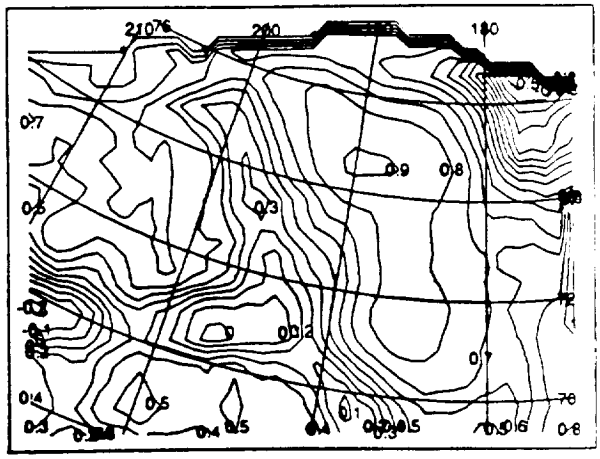

Latitude

Longitude
Ross Sea 8/15/1983

Ice Concentrations

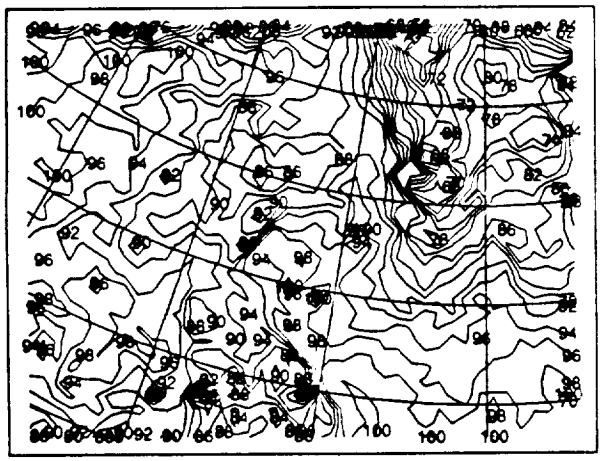

Latitude

Longitude
Ross Sea 10/14/1983

Local Correlations

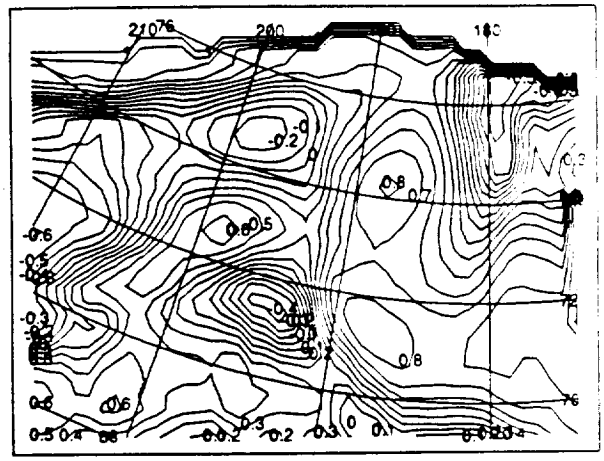

Latitude

Longitude
Ross Sea 10/14/1983

Ice Concentrations

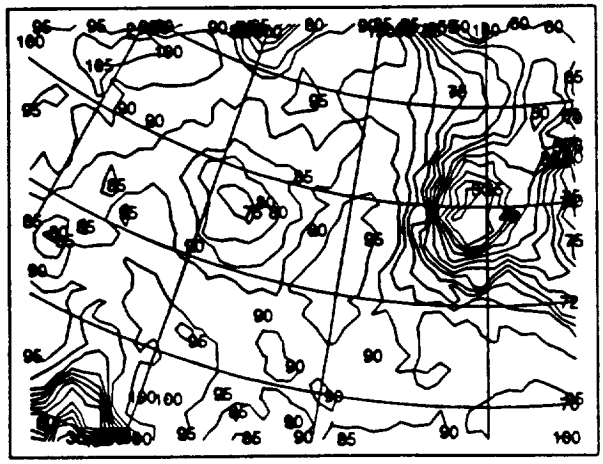

Latitude

Longitude
Ross Sea 11/19/1983

Local Correlations

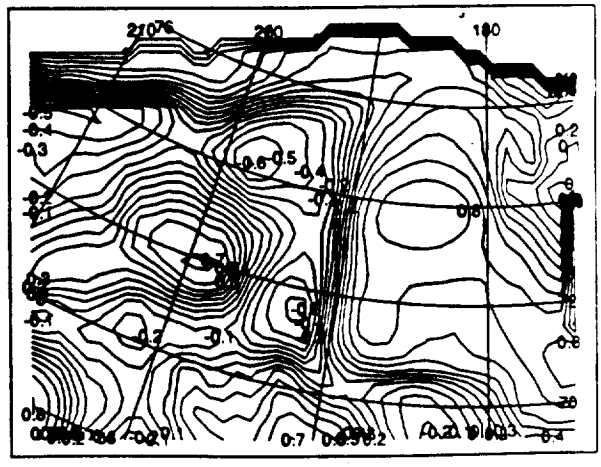

Latitude

Longitude
Ross Sea 11/19/1983

Figure 8.d

Ice Concentrations

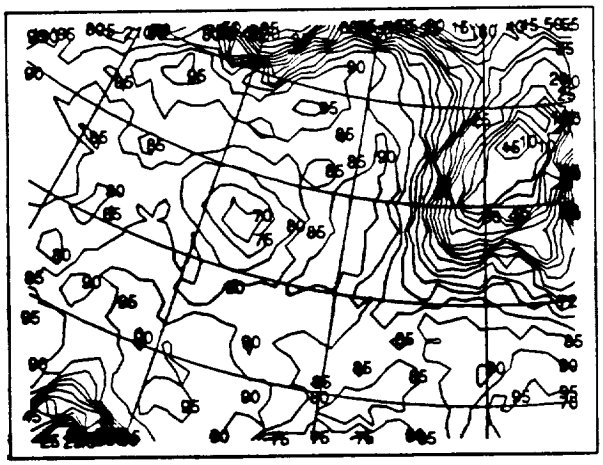

Latitude

Longitude
Ross Sea 11/23/1983

Local Correlations

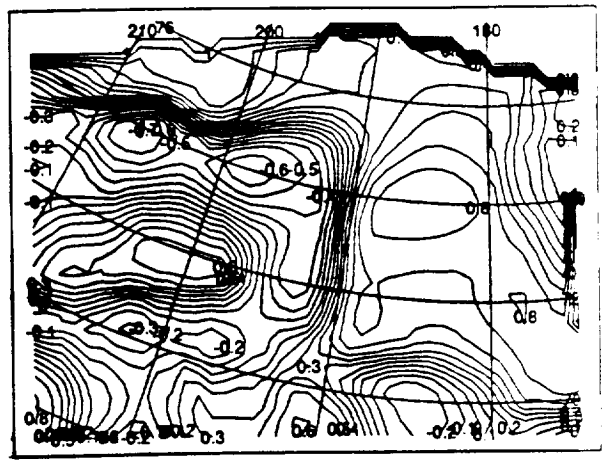

Latitude

Longitude
Ross Sea 11/23/1983

Ice Concentrations

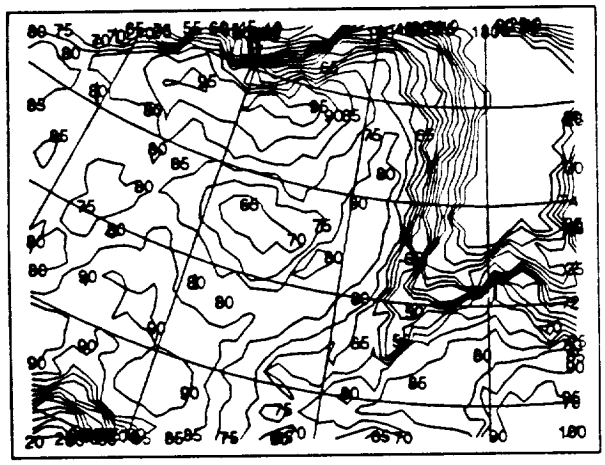

Latitude

Longitude
Ross Sea 11/27/1983

Local Correlations

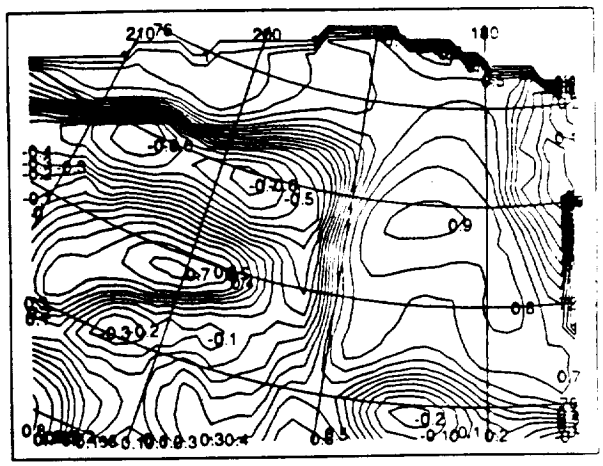

Latitude

Longitude
Ross Sea 11/27/1983

Ice Concentrations

Latitude

Longitude
Ross Sea 12/1/1983

Local Correlations

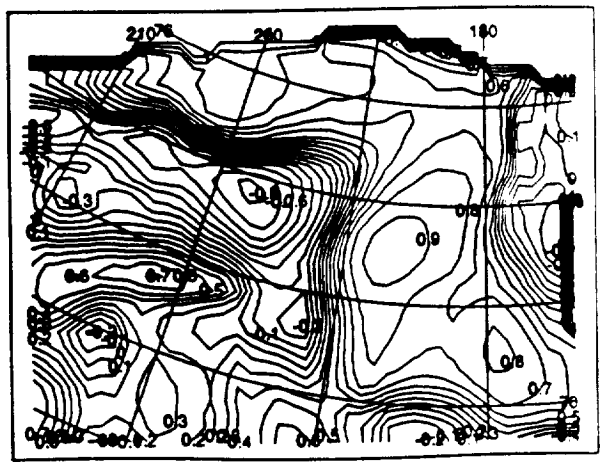

Latitude

Longitude
Ross Sea 12/1/1983

Figure 8.e

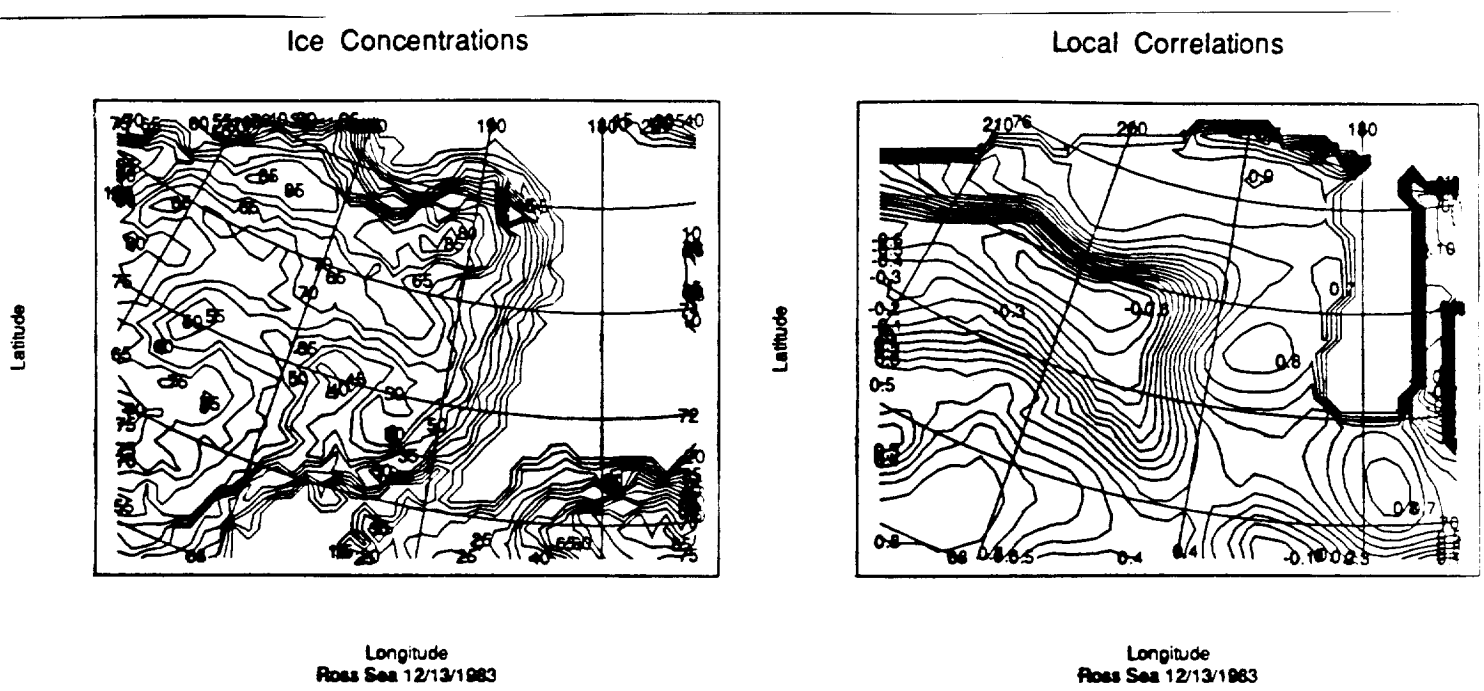
Ice Concentrations
Local Correlations
Latitude
Latitude
Longitude
Ross Sea 12/13/1983
Longitude
Ross Sea 12/13/1983

Figure 8.f

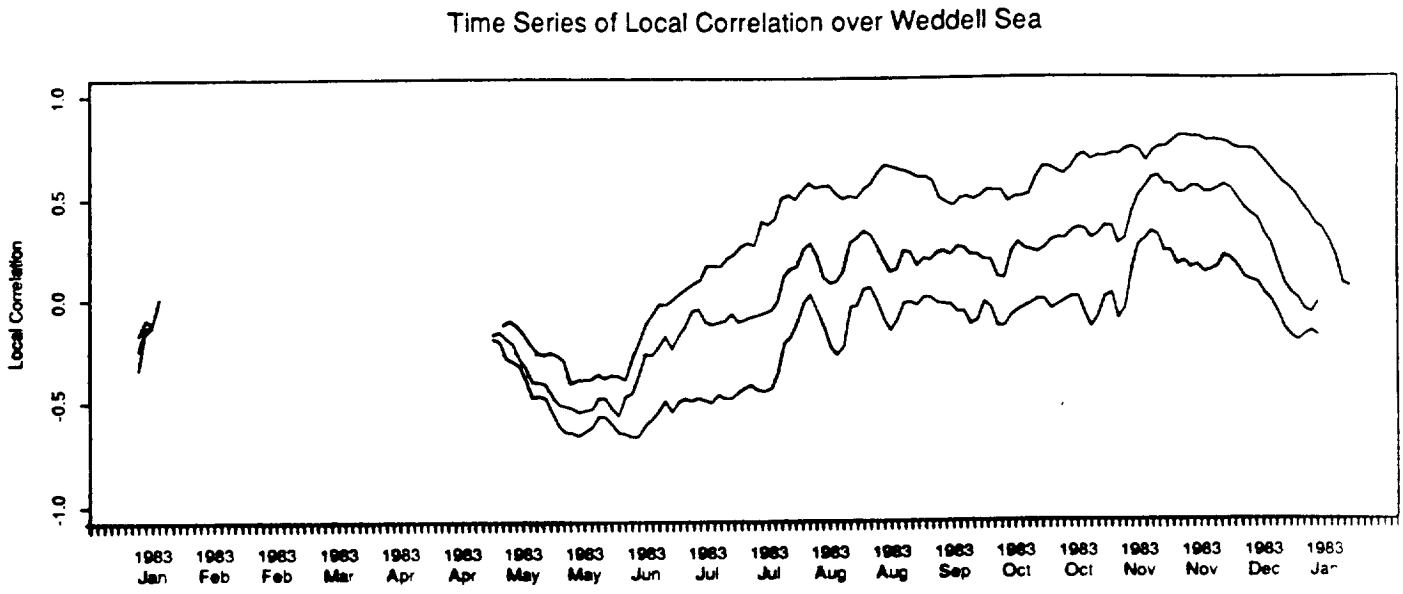
Time Series of Local Correlation over Weddell Sea
Local Correlation
1.0
0.5
0.0
-0.5
-1.0
1983 Jan
1983 Feb
1983 Feb
1983 Mar
1983 Apr
1983 Apr
1983 May
1983 May
1983 Jun
1983 Jul
1983 Jul
1983 Aug
1983 Aug
1983 Sep
1983 Oct
1983 Oct
1983 Nov
1983 Nov
1983 Dec
1983 Jan

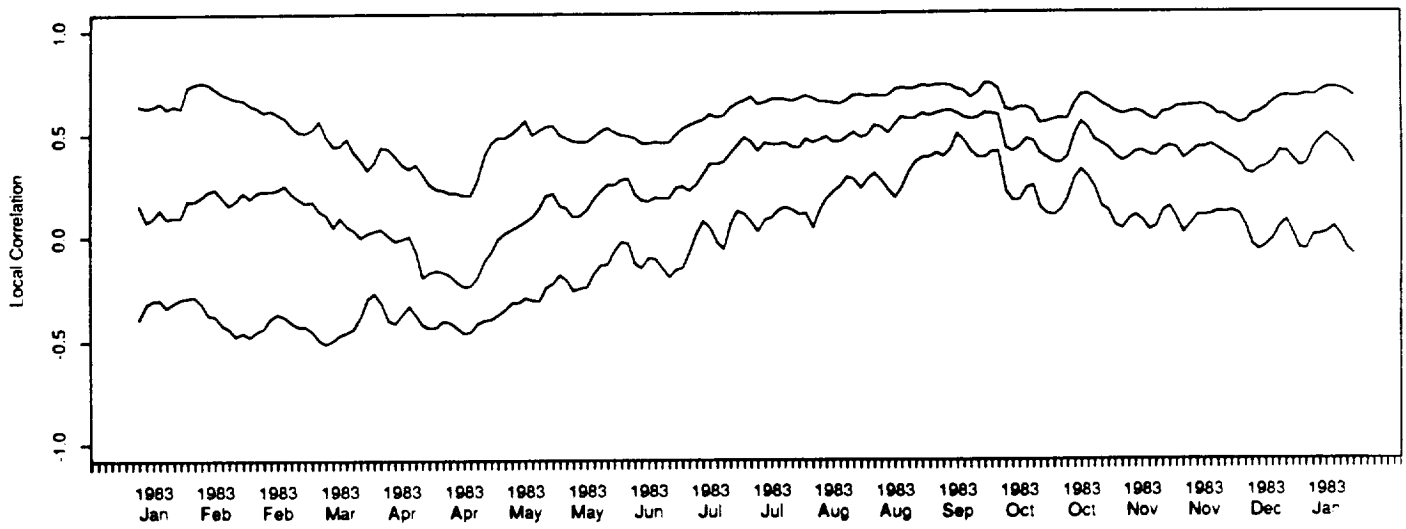
Time Series of Local Correlation over Ross Sea
Local Correlation
1.0
0.5
0.0
-0.5
-1.0
1983 Jan
1983 Feb
1983 Feb
1983 Mar
1983 Apr
1983 Apr
1983 May
1983 May
1983 Jun
1983 Jul
1983 Jul
1983 Aug
1983 Aug
1983 Sep
1983 Oct
1983 Oct
1983 Nov
1983 Nov
1983 Dec
1983 Jan

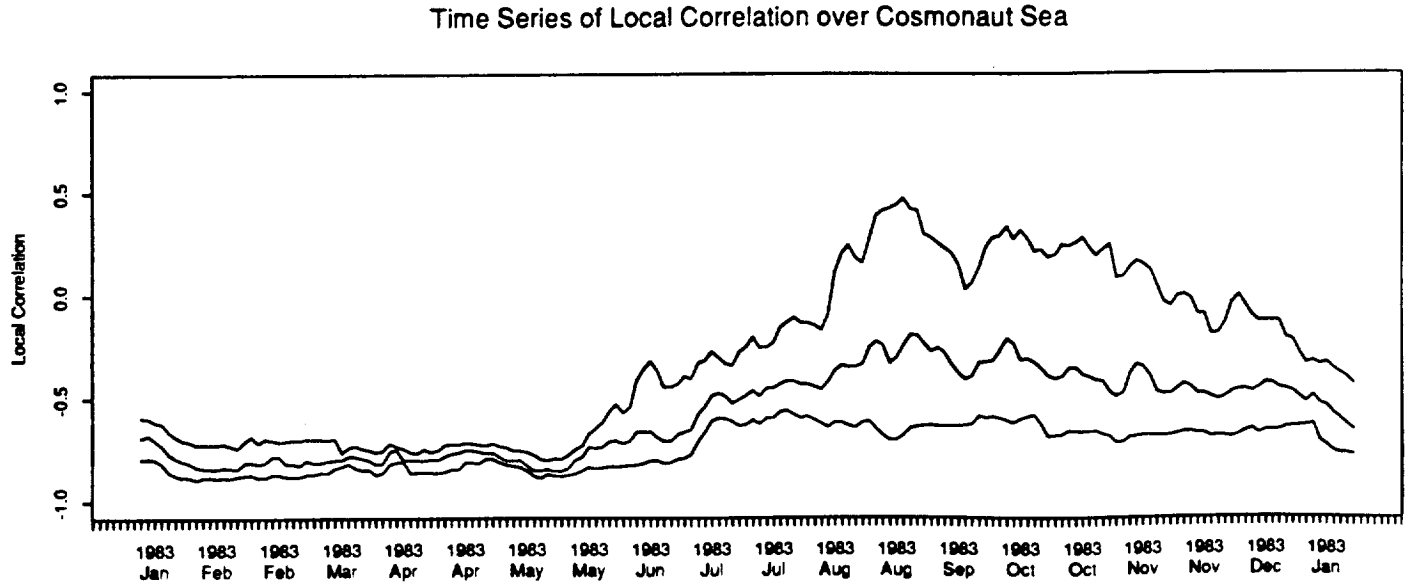
Time Series of Local Correlation over Cosmonaut Sea
Local Correlation
1.0
0.5
0.0
-0.5
-1.0
1983 Jan
1983 Feb
1983 Feb
1983 Mar
1983 Apr
1983 Apr
1983 May
1983 May
1983 Jun
1983 Jul
1983 Jul
1983 Aug
1983 Aug
1983 Sep
1983 Oct
1983 Oct
1983 Nov
1983 Nov
1983 Dec
1983 Jan

Figure 9

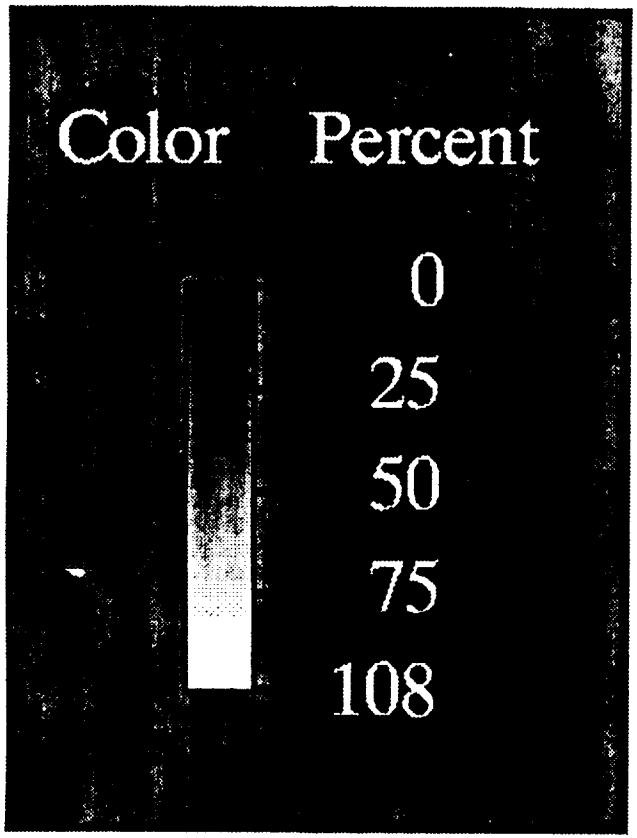
Color
Percent
0
25
50
75
108

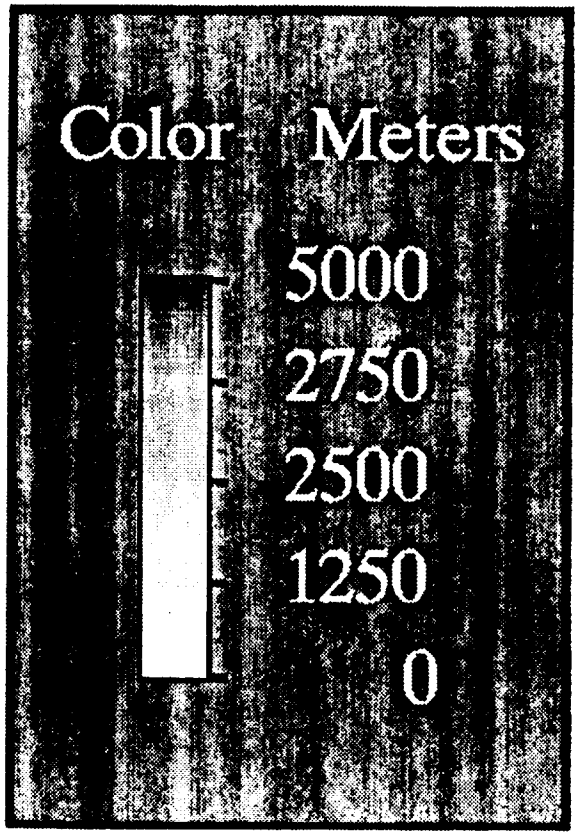
Color
Meters
5000
2750
2500
1250
0

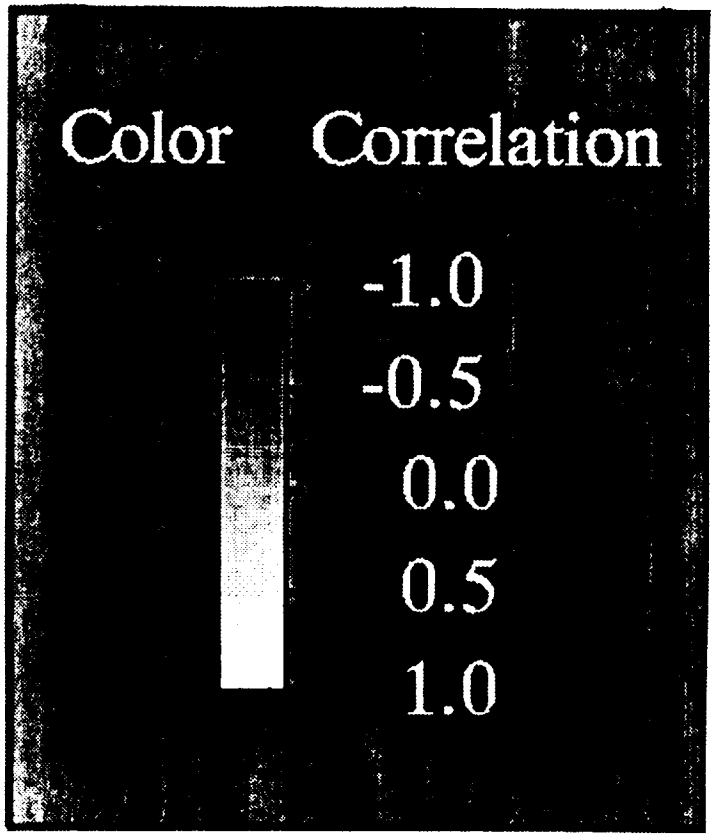
Color
Correlation
-1.0
-0.5
0.0
0.5
1.0

Exhibit 1